JOURNAL OF GEOPHYSICAL RESEARCH, VOL. 112, G03013, doi:10.1029/2006JG000282, 2007



# Partitioning net ecosystem exchange of $CO_2$: A comparison of a Bayesian/isotope approach to environmental regression methods

J. M. Zobitz,[1] S. P. Burns,[2] J. Ogée,[3] M. Reichstein,[4] and D. R. Bowling[5]

Received 1 August 2006; revised 29 May 2007; accepted 6 July 2007; published 6 September 2007.

[1] Separation of the net ecosystem exchange of $CO_2$ ($F$) into its component fluxes of net photosynthesis ($F_A$) and nonfoliar respiration ($F_R$) is important in understanding the physical and environmental controls on these fluxes, and how these fluxes may respond to environmental change. In this paper, we evaluate a partitioning method based on a combination of stable isotopes of $CO_2$ and Bayesian optimization in the context of partitioning methods based on regressions with environmental variables. We combined high-resolution measurements of stable carbon isotopes of $CO_2$, ecosystem fluxes, and meteorological variables with a Bayesian parameter optimization approach to estimate $F_A$ and $F_R$ in a subalpine forest in Colorado, United States, over the course of 104 days during summer 2003. Results were generally in agreement with the independent environmental regression methods of Reichstein et al. (2005a) and Yi et al. (2004). Half-hourly posterior parameter estimates of $F_A$ and $F_R$ derived from the Bayesian/isotopic method showed a strong diurnal pattern in both, consistent with established gross photosynthesis (*GEE*) and total ecosystem respiration (*TER*) relationships. Isotope-derived $F_A$ was functionally dependent on light, but $F_R$ exhibited the expected temperature dependence only when the prior estimates for $F_R$ were temperature-based. Examination of the posterior correlation matrix revealed that the available data were insufficient to independently resolve all the Bayesian-estimated parameters in our model. This could be due to a small isotopic disequilibrium ($\mathcal{D}$) between $F_A$ and $F_R$, poor characterization of whole-canopy photosynthetic discrimination or the isotopic flux (isoflux, analogous to net ecosystem exchange of $^{13}CO_2$). The positive sign of $\mathcal{D}$ indicates that $F_A$ was more enriched in $^{13}C$ than $F_R$. Possible reasons for this are discussed in the context of recent literature.

**Citation:** Zobitz, J. M., S. P. Burns, J. Ogée, M. Reichstein, and D. R. Bowling (2007), Partitioning net ecosystem exchange of $CO_2$: A comparison of a Bayesian/isotope approach to environmental regression methods, *J. Geophys. Res.*, *112*, G03013, doi:10.1029/2006JG000282.

## 1. Introduction

[2] Carbon uptake by terrestrial ecosystems is estimated at 2–4 Gt C/yr and therefore constitutes a crucial component of the global carbon cycle [*Schimel et al.*, 2001]. Large uncertainties still remain regarding the latitudinal patterns of the net $CO_2$ uptake [*Piovesan and Adams*, 2000; *Valentini et al.*, 2000; *Janssens et al.*, 2001; *Schimel et al.*, 2001; *Van Dijk and Dolman*, 2004] and uptake in response to climate variations [*Goulden et al.*, 1996; *Huxman et al.*, 2003; *Davidson et al.*, 2006; *Ciais et al.*, 2005]. These uncertainties reflect the complexity in how environmental drivers affect gross photosynthesis (*GEE*) and total ecosystem respiration (*TER*). In order to resolve these uncertainties, a better understanding of the underlying biological processes is clearly needed.

[3] In the absence of any disturbance, the net ecosystem $CO_2$ exchange between terrestrial ecosystems and the atmosphere (*NEE*, noted $F$ here using the notation of *Bowling et al.* [2003a]; see Table 1 for a full listing of all abbreviations used in the text) is the sum of two opposing fluxes *GEE* and *TER*: $F = GEE + TER$, where $GEE < 0$ and $TER > 0$. For an isotope-based approach, foliar respiration ($F_L$) is often excluded from *TER* and included into net photosynthesis, ($F_A = GEE + F_L$) so that $F = F_A + F_R$, where $F_R$ denotes nonfoliar respiration ($F_R = TER - F_L$) [*Lloyd et al.*, 1996]. Net ecosystem exchange is measured with the

[1]Department of Mathematics, University of Utah, Salt Lake City, Utah, USA.
[2]Department of Ecology and Evolutionary Biology (EEB), University of Colorado, Boulder, Colorado, USA.
[3]EPHYSE (Functional Ecology and Environmental Physics), INRA, BP 81, Villenave d'Ornon, France.
[4]Biogeochemical Model-Data Integration Group, Max-Planck Institute for Biogeochemistry, Jena, Germany.
[5]Department of Biology, University of Utah, Salt Lake City, Utah, USA.


0148-0227/07/2006JG000282$09.00

eddy covariance technique and is the sum of a turbulent flux ($F_{eddy}$) and storage flux ($F_{storage}$) [*Wofsy et al.*, 1993].

$$F_A + F_R = \overline{w' C_a'} + \int_0^{z_h} \frac{dC_a}{dt} dz = F_{eddy} + F_{storage} = F \quad (1)$$

In equation (1), $w'$ is the vertical turbulent wind speed (m $s^{-1}$), $C_a'$, turbulent fluctuation of $CO_2$ molar density ($\mu$mol $m^{-3}$), $z_h$ the flux measurement height, $C_a$ the molar density of atmospheric $CO_2$ ($\mu$mol $m^{-3}$). $F$, $F_A$, and $F_R$ have units $\mu$mol $CO_2$ $m^{-2}$ $s^{-1}$. $F$ is measured worldwide at more than 400 sites in a variety of biomes through the FLUXNET network (http://www.fluxnet.ornl.gov/fluxnet) [*Baldocchi et al.*, 2001].

[4] Separating $F$ into its constituent fluxes of $F_A$ and $F_R$ (or *GEE* and *TER*) is termed *flux partitioning*. This partitioning can be done via statistical parameter estimation using $F$ and climatic variables (e.g., temperature, light, moisture) as covariates [*Huxman et al.*, 2003; *Yi et al.*, 2004; *Reichstein et al.*, 2005a], combining $F$ with process-based biophysical models [*Aber et al.*, 1996; *Baldocchi and Bowling*, 2003; *Ogée et al.*, 2003a; *Dai et al.*, 2004; *Braswell et al.*, 2005; *Sacks et al.*, 2006; *Stoy et al.*, 2006], scaling chamber measurements to the ecosystem [*Lavigne et al.*, 1997; *Law et al.*, 1999], or, as in this study, with stable isotopes of $CO_2$ [*Yakir and Wang*, 1996; *Bowling et al.*, 2001, 2003a; *Ogée et al.*, 2003b, 2004; *Lai et al.*, 2004; *Knohl and Buchmann*, 2005; *Griffis et al.*, 2005; *Zhang et al.*, 2006].

[5] Each of these flux partitioning routines have advantages and disadvantages associated with their use. For example, statistical parameter estimation of $F$ with climatic variables uses expected physiological patterns (e.g., *TER* exponentially related to temperature) and determines unknown functional parameters to find a best estimate of $F$ [*Huxman et al.*, 2003; *Yi et al.*, 2004; *Reichstein et al.*, 2005a]. The advantage to this approach is that relatively few parameters (usually 2–4) are needed to characterize the functional relationships and there are plentiful data observations (usually 48 daily measurements of $F$) to characterize such relationships. However, if nighttime $F$ measurements are used to determine a functional relationship for *TER*, in times of strong atmospheric stability $F_{eddy}$ may not be estimated correctly [*Goulden et al.*, 1996], potentially biasing the estimate of *TER*. Recent literature has addressed the appropriateness of scaling respiration with temperature, as ecosystem respiration is expected to vary with other environmental factors such as moisture or substrate availability [*Giardina and Ryan*, 2000; *Reichstein et al.*, 2005b; *Davidson et al.*, 2006; *Davidson and Janssens*, 2006]. Moreover, temperature-flux relationships are derived from seasonal flux data and thus do not necessarily reflect the diurnal temperature-flux relationships. Recent work by *Reichstein et al.* [2005a] has attempted to address these disadvantages by removing periods of atmospheric stability, utilizing a sophisticated gap-filling routine, and using only 15-day periods to derive the temperature-flux relationship.

[6] Scaling chamber measurements up to the ecosystem is difficult due to problems of spatial representativeness and establishment of labor-intensive allometric relationships. *Lavigne et al.* [1997] scaled chamber-based respiration measurements to the ecosystem and found that nighttime $F$ measurements were consistently lower by 20–40%.

[7] Biophysical models allow estimation of biological processes in the absence of direct measurements, however these processes require a large number of additional parameters to describe them [*Braswell et al.*, 2005; *Sacks et al.*, 2006]. We ultimately want to test and improve models with partitioned flux estimates from other alternative methods.

[8] Stable isotopes of $CO_2$ provide measurements to characterize another flux partitioning method. Unlike environmental regression methods, the isotope flux partitioning method does not assume that $F_R$ is dependent on temperature or that $F_A$ depends on incoming radiation. Hence, isotope-partitioned fluxes can be used to test these relationships at the ecosystem scale. An additional advantage to the isotope method is that it provides information about the isotopic signatures of net photosynthesis ($F_A$) and nonfoliar respiration ($F_R$). These isotopic signatures can be used to infer information about ecosystem physiology and the relations between carbon and water vapor fluxes. A fundamental requirement of the isotopic method is that the isotopic signature of carbon products associated with nonfoliar respiration ($\delta_R$) is different from the isotopic signature of carbon products associated with net photosynthesis ($\delta_A$). Using mass balance of $^{13}CO_2$, one can derive an equation that represents net ecosystem exchange of $^{13}CO_2$ [*Yakir and Wang*, 1996; *Lloyd et al.*, 1996; *Raupach*, 2001; *Bowling et al.*, 2001, 2003a]:

$$\delta_A F_A + \delta_R F_R = F_{eddy-isoflux} + F_{isostorage} = F_\delta, \quad (2)$$

where $F_A$, $F_R$, $\delta_A$ (‰), and $\delta_R$ (‰) are defined above, $F_{eddy-isoflux}$ ($\mu$mol $m^{-2}$ $s^{-1}$ ‰) is the eddy isoflux, and $F_{isostorage}$ ($\mu$mol $m^{-2}$ $s^{-1}$ ‰) is the isotopic storage flux. In addition to $F$, the isotope partitioning method requires measurements of $F_\delta$, [$CO_2$], and $\delta^{13}C$. See the Appendix in *Bowling et al.* [2003a] for the full derivation of equations (1) and (2) and the approximations used to attain them. Carbon isotope ratios ($\delta^{13}C_X$ or $\delta_X$) are calculated in the usual manner as the deviation of a $^{13}CO_2$ to $^{12}CO_2$ ratio in sample $X$ from an international standard (Vienna PDB). The deviation of this ratio from unity is expressed as permil (‰). Using the permil notation, the isoflux ($F_\delta$) is analogous to the net ecosystem exchange of $^{13}CO_2$ and has units of ‰ $\mu$mol $CO_2$ $m^{-2}$ $s^{-1}$ rather than $\mu$mol $^{13}CO_2$ $m^{-2}$ $s^{-1}$ [*Bowling et al.*, 2003a]. With equations (1) and (2), one has a set of linear equations to determine $F_A$ and $F_R$.

[9] A disadvantage to the isotope partitioning method is that the difference between $\delta_A$ and $\delta_R$ can be near zero. The difference between $\delta_A$ and $\delta_R$ is defined as the isotopic disequilibrium: $\mathcal{D} = \delta_A - \delta_R$. Note that when $\mathcal{D} \approx 0$ ($\delta_A \approx \delta_R$), there is no unique information in equation (2) relative to equation (1). This violates the fundamental requirement of the method that photosynthesis and respiration are isotopically different. Therefore when $\mathcal{D} = 0$ this implies that stable carbon isotope measurements do not contain unique information about $F_A$ and $F_R$ distinct from $F$.

[10] A practical limitation of the isotope partitioning method is the collection of enough data to resolve diurnal signals of $\delta^{13}C$ ratios. *Ogée et al.* [2004] conducted an intensive campaign of flask-based collection of [$CO_2$] in

**Table 1.** List of Symbols and Variables Used in Text

| Symbol | Units | Description |
|---|---|---|
| $C_a$ | $\mu$mol m$^{-3}$ | $CO_2$ molar density |
| $w'$ | m s$^{-1}$ | Turbulent component to vertical wind speed |
| $C_a{}'$ | $\mu$mol m$^{-3}$ | Turbulent component to $CO_2$ molar density |
| $z_h$ | m | Reference height (21.5 m) |
| $F_{eddy}$ | $\mu$mol m$^{-2}$ s$^{-1}$ | Turbulent eddy flux, defined by $\overline{w'C_a'}$ |
| $F_{storage}$ | $\mu$mol m$^{-2}$ s$^{-1}$ | Storage $CO_2$ flux, see equation (1) |
| $F$ | $\mu$mol m$^{-2}$ s$^{-1}$ | Net ecosystem exchange of $CO_2$, defined by equation (1) |
| $GEE$ | $\mu$mol m$^{-2}$ s$^{-1}$ | Gross primary production flux |
| $TER$ | $\mu$mol m$^{-2}$ s$^{-1}$ | Total ecosystem respiration flux |
| $F_A$ | $\mu$mol m$^{-2}$ s$^{-1}$ | Net ecosystem photosynthetic flux of $CO_2$ (gross primary production less foliar respiration) |
| $F_R$ | $\mu$mol m$^{-2}$ s$^{-1}$ | Ecosystem heterotrophic respiration |
| $F_L$ | $\mu$mol m$^{-2}$ s$^{-1}$ | Ecosystem foliar respiration |
| $T_0$ | °C | Regression parameter for TER relationship, see equation (11) (−46°C) |
| $T_{Ref}$ | °C | Reference temperature, see equation (11) (10°C) |
| $R_{ref}$ | $\mu$mol m$^{-2}$ s$^{-1}$ | Reference respiration rate, see equation (11) |
| $E_0$ | C | Activation energy, see equation (11) |
| $\alpha_1(T)$ | dimensionless | Parameter in *GEE* functional form for *Yi et al.* [2004], see equation (13) |
| $\alpha_2(T)$ | $\mu$mol m$^{-2}$ s$^{-1}$ | Parameter in *GEE* functional form for *Yi et al.* [2004], see equation (13) |
| $Q_P$ | $\mu$mol m$^{-2}$ s$^{-1}$ | Photosynthetically active radiation |
| $\Delta_{canopy}$ | ‰ | Flux-weighted canopy-scale photosynthetic carbon isotope discrimination |
| $\delta_a$ | ‰ | Observed isotope ratio at a given measurement height (0.1–21.5 m) |
| $c_a$ | ppm | Observed [$CO_2$] mixing ratio at a given measurement height (0.1–21.5 m) |
| $\delta_B$ | ‰ | Background isotope ratio, see equations (5) |
| $c_B$ | ppm | Background [$CO_2$] mixing ratio, see equations (5) |
| $\delta_R$ | ‰ | Isotope ratio of nighttime $F$, assumed to be the isotope ratio of daytime $F_R$, see equation (5) |
| $\delta_N$ | ‰ | Isotope ratio of daytime $CO_2$ flux, see equation (6) |
| $\phi$ | ‰ ppm | Slope of a nighttime isotopic mixing line, see equation (5) |
| $\beta$ | ‰ ppm | Slope of a daytime isotopic mixing line, see equation (6) |
| $\overline{\delta a}$ | ‰ | Average isotope ratio of 5, 7, 9, 11 m canopy air |
| $\overline{c}_a$ | ppm | Average [$CO_2$] mixing ratio of 5, 7, 9, 11 m canopy air |
| $F_{isostorage}$ | $\mu$mol m$^{-2}$ s$^{-1}$ ‰ | Isotopic storage flux, expressed in ‰ notation, see equation (2) |
| $F_\delta$ | $\mu$mol m$^{-2}$ s$^{-1}$ ‰ | Net ecosystem exchange of $^{13}CO_2$, expressed in ‰ notation, see equation (2) |
| $g_a$ | mol m$^{-2}$ s$^{-1}$ | Aerodynamic conductance to [$CO_2$] |
| $g_s$ | mol m$^{-2}$ s$^{-1}$ | Surface conductance to [$CO_2$] |
| $g_m$ | mol m$^{-2}$ s$^{-1}$ | Mesophyll conductance to [$CO_2$] (constant at 0.125 mol m$^{-2}$ s$^{-1}$) |
| $\overline{g}$ | mol m$^{-2}$ s$^{-1}$ | Overall conductance of [$CO_2$], see equation (8) |
| $c_c$ | ppm | [$CO_2$] mixing ratio at the sites of carboxylation |
| $a_b$ | ‰ | Leaf boundary layer fractionation (2.9‰) |
| $a$ | ‰ | Diffusion fractionation (4.4‰) |
| $a_s(T)$ | ‰ | Water dissolution fractionation (1.1‰) |
| $a_1$ | ‰ | Mesophyll diffusion fractionation (0.7‰) |
| $\overline{a}$ | ‰ | Overall photosynthetic fractionation |
| $b_R$ | ‰ | Photosynthetic enzymatic fractionation of $^{13}CO_2$ (27.5‰) |
| $\mathcal{D}$ | ‰ | Isotopic disequilibrium, equals $\delta_A - \delta_R$ |
| $\vec{m}_{prior}$ | variable | Prior parameter vector |
| $C_M$ | variable | Prior parameter covariance matrix |
| $\vec{d}$ | variable | Data vector |
| $C_D$ | variable | Data covariance matrix |
| $G$ | variable | Model relating parameters $\vec{m}$ to data $\vec{d}$ |
| $\vec{m}*$ | variable | Posterior Bayesian parameter vector, see equation (17) |
| $\tilde{C}_M$ | variable | Posterior Bayesian parameter covariance matrix, see equation (18) |
| $E$ | variable | Posterior correlation matrix, see equation (19) |

canopy air analyzed by a mass spectrometer for $\delta^{13}C$ ratios. Such measurement campaigns traditionally have been the only way to resolve diurnal signals of $\delta^{13}C$ ratios needed for isotopic partitioning [*Schauer et al.*, 2003; *Ogée et al.*, 2003b; *Knohl and Buchmann*, 2005]. The advent of tunable diode laser (TDL) spectroscopy has alleviated this limitation and continuous measurements of [$CO_2$] mixing ratios and $\delta^{13}C$ ratios can now be made in the field [*Bowling et al.*, 2003b; *Griffis et al.*, 2004; *Bowling et al.*, 2005; *Griffis et al.*, 2005; *Zhang et al.*, 2006].

[11] Mathematical techniques such as Bayesian parameter estimation provide a tool to account for additional information (such as reasonable bounds for values of $F_A$ and $F_R$) beyond process models such as equations (1) and (2). Hence Bayesian parameter estimation can be applied to extract information about ecosystem-scale fluxes from high-resolution measurements of $F$, [$CO_2$], and $\delta^{13}C$. This technique is gaining popularity in the environmental science community as a way to extract meaningful information from the inherent stochasticity in environmental observations [*Clark*, 2005; *Raupach et al.*, 2005]. Bayesian parameter estimation can be used to estimate parameters that drive biophysical models [*Braswell et al.*, 2005; *Knorr and Kattge*, 2005; *Sacks et al.*, 2006; *Xu et al.*, 2006], estimate surface/ocean fluxes from global flask measurements [*Bousquet et al.*, 1999; *Peters et al.*, 2005], estimate anthropogenic sources of [$CO_2$] using high-resolution stable isotope measurements [*Pataki et al.*, 2006], or as we focus in this paper, isotope flux partitioning of $F$ from $CO_2$ and $^{13}C$ measurements in forest air. One of the ways that Bayesian parameter estima-

tion directly contrasts with traditional parameter estimation is the use of prior information for the target parameters [*Jaynes*, 2003]. This prior information provides a way to account for additional information about parameters (such as reasonable probability distributions for $F_A$ and $F_R$) that cannot be specified in the model.

[12] *Ogée et al.* [2004] used Bayesian parameter estimation in conjunction with isotope flux partitioning at a homogeneous maritime forest in France. A major conclusion of *Ogée et al.* [2004] was that the utility of the isotope partitioning approach was limited by values of $\mathcal{D}$ near zero. In this study, we address two primary questions motivated from the study of *Ogée et al.* [2004]. First, do we find $\mathcal{D} \approx 0$ using a high-resolution data set of $F$, $[CO_2]$, and $\delta^{13}C$ collected in a heterogeneous high-elevation forest? Second, if $\mathcal{D}$ is near zero, then what biological processes influence $\mathcal{D}$ being near zero?

[13] To address these questions, this study utilizes a three-month data set of measurements collected at a high-elevation subalpine forest in Colorado (the Niwot Ridge AmeriFlux size). We apply the isotope partitioning method with Bayesian parameter estimation to examine photosynthesis, respiration, and isotope disequilibrium. For this study, we specifically address the following objectives:

[14] 1. Expand upon the approach of *Ogée et al.* [2004] and apply a Bayesian optimization method to isotope flux partitioning. For this approach the estimated parameters include $F_A$, $F_R$, and $\delta_A$.

[15] 2. Attempt to independently resolve the parameters $F_A$, $F_R$, and $\delta_A$ from prior information of these parameters.

[16] 3. Identify mathematical and biological factors that might limit the effective application of Bayesian parameter estimation to isotope flux partitioning based upon the results of the previous two objectives.

[17] The third objective assesses how the mathematical and biological techniques influence the interpretation of the partitioned fluxes. If the isotope flux partitioning method is to be used to develop ecosystem-scale functional relationships, it is critically important to understand how these estimates of $F_A$ and $F_R$ are derived. Hence our guiding philosophy was to use a process model and a Bayesian parameter estimation technique that allowed us to investigate the direct effects of how the process model and Bayesian parameter estimation technique influence the final parameter estimates.

[18] From this data set of $F$, $[CO_2]$, and $\delta^{13}C$, this study generates half-hourly Bayesian parameter estimates of $F_A$ and $F_R$ and other additional parameters. We do not include correlations of the parameters between time steps because of the synchronicity of $[CO_2]$ and $\delta^{13}C$ data at all daytime measurement levels (see Figure 2 in *Bowling et al.* [2005]). From these Bayesian parameter estimates, we then compare the posterior results to expected canopy physiological relationships and discuss the sensitivity of posterior parameter estimates to prior assumptions. Finally, we make recommendations on where our understanding of process-based ecosystem parameters can be improved.

## 2. Site Description and Measurements

[19] This study was conducted at the Niwot Ridge AmeriFlux site, a subalpine forest at 3050 m elevation west of Boulder, Colorado (40°1′58″N; 105°32′46″W). The site is a century-old forest, recovering from early twentieth century logging. The forest contains subalpine fir (*Abies lasiocarpa*), Engelmann spruce (*Picea engelmannii*), and lodgepole pine (*Pinus contorta*). Canopy height is 11–12 m. Mean annual precipitation averages 800 mm and the mean annual temperature is 1.5°C [*Monson et al.*, 2002].

[20] Mean $CO_2$ profiles (for the term $F_{storage}$ in equation (1)) were measured with a closed-path infrared gas analyzer (IRGA) (LI-COR Inc., Lincoln, Nebraska, model LI-6251) that used a magnesium perchlorate trap to remove water vapor from the air sample. Fluctuations of $CO_2$ and water vapor were measured with a second closed-path IRGA (LI-COR, model LI-6262) where the measured $CO_2$ was corrected for the pressure-broadening and dilution effects of water vapor as described in the LI-6262 manual. While we have conveniently represented $F_{eddy}$ as $\overline{w'C'_a}$ in equation (1), it should be noted that $F_{eddy}$ includes the effect of water vapor fluctuations on $\overline{w'C'_a}$ (i.e., the so-called "Webb correction" or WPL term for flux calculations [*Webb et al.*, 1980]). During the summer, the water-vapor WPL term at Niwot Ridge is small at night, but during the day it can be on the order of 30% of $F_{eddy}$. Temperature fluctuations have been minimized by passing the air sample through a short length of copper tubing prior to entering the LI-6262 sample cell. Additional details about the eddy covariance and meteorological measurements at Niwot Ridge can be found in *Monson et al.* [2002]. Prevailing winds at Niwot Ridge occur from the west; *Turnipseed et al.* [2003] conservatively estimated that 90% of a flux measurement originates from 1200m west of the tower. Additional details about the footprint of a flux measurement can be found in that study.

[21] Carbon dioxide mixing ratios and $\delta^{13}C$ ratios were made over three consecutive summer months in 2003 (4 July–15 October, day of year 185–288) by tunable diode laser absorption (TDL) spectrometry as detailed in *Bowling et al.* [2005]. Measurements at nine canopy heights (0.1, 0.5, 1, 2, 5, 7, 9, 11, and 21.5 m) were made every six minutes. This six minute data was then averaged into half-hourly values for use in our analysis. Uncertainties associated with $[CO_2]$ and $\delta^{13}C$ measurements were 0.15 ppm and 0.15‰. See *Bowling et al.* [2005] for additional description on how these uncertainties were determined.

[22] During the study period, average daytime temperatures were 12°C, with minimum and maximum values ranging from −6 to 26°C. Average vapor pressure deficit was 1 kPa but ranged from minimum and maximum values of 0–2.6 kPa. The study period had frequent late-afternoon rain events yielding small amounts of precipitation. The maximum period between rain events lasted two weeks from September 18 to October 1 and the highest precipitation rain event (20 mm) occurred August 30.

[23] Figure 1 shows the diurnal histograms of available data. Quality control measures led to a 10 day gap from days 200–210 due to failure of the ground heat flux measurement (necessary in the calculation of $\overline{g}$, see section 4.1) and a 20 day period from days 240–260 where $F$ was gap-filled. Additional time periods were removed in times when the atmosphere was strongly stable [*Goulden et al.*, 1996]. Poor calibration performance with the TDL at midday further reduced periods available for partitioning. Of all possible daytime half-hourly periods, 34% were

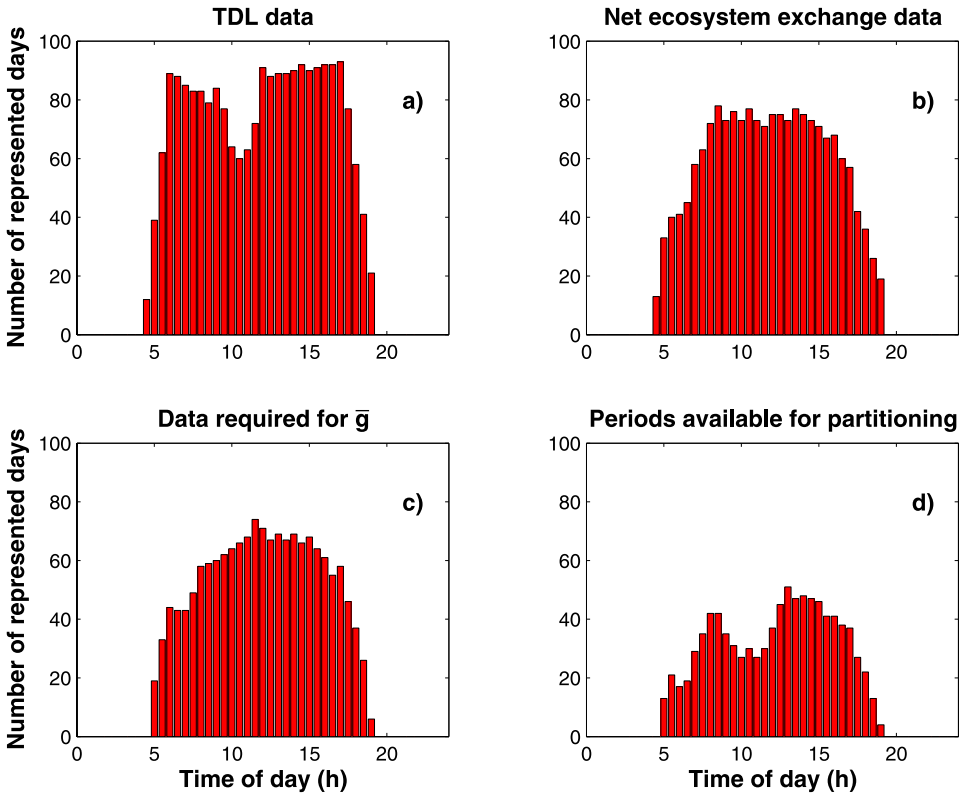


**Figure 1.** Diurnal representation of available daytime data from 4 July to 15 October 2003 (104 days) at the Niwot Ridge AmeriFlux site, as described by the quality control measures in section 2. The vertical axis represents the number of measurements for a particular half-hour period. Data availability at night is not shown in the figure.

available to be partitioned (942 out of 2754 possible half-hourly periods).

## 3. Theory

### 3.1. Isotopic Partitioning Method

[24] Equations (1) and (2) define conservation of $CO_2$ and $^{13}CO_2$ and have previously been discussed. These equations are expanded in equations (3) and (4), with the difference that $\delta_A$, the isotopic signature of photosynthetic products, is expressed as the difference between the average isotope ratio of canopy air ($\overline{\delta}_a$) and whole canopy photosynthetic discrimination $\Delta_{canopy}$ [*Bowling et al.*, 2001, 2003a].

$$F_A + F_R = F_{eddy} + F_{storage} \tag{3}$$

$$(\overline{\delta}_a - \Delta_{canopy})F_A + \delta_R F_R = F_{eddy-isoflux} + F_{isostorage} = F_\delta \tag{4}$$

[25] The isotopic content of ecosystem respiration ($\delta_R$) can be derived from nighttime [$CO_2$] and $\delta^{13}C$ measurements. Since photosynthesis only occurs in the light, during the night there is a net flux of respiratory carbon from the ecosystem. Using mass conservation equations for total $CO_2$ and $^{13}CO_2$, the following "Keeling-plot" equation can be derived [*Keeling*, 1958]:

$$\delta_a = c_B \frac{(\delta_B - \delta_R)}{c_a} + \delta_R = \frac{\phi}{c_a} + \delta_R \qquad \text{(night)}, \tag{5}$$

where $\phi$ (‰ ppm) is the slope of the nighttime Keeling plot, $c_a$ (ppm) is the total measured [$CO_2$], $c_B$ (ppm) is the background [$CO_2$] and $\delta_a$ (‰) and $\delta_B$ (‰) are defined analogously. For this study we assume that values of $\delta_R$ are constant during the day. This assumption is not correct as studies have shown components of $\delta_R$ to be quite dynamic during the daytime [*Hymus et al.*, 2005; *Prater et al.*, 2006]. This assumption is discussed further in section 5.1.

[26] Shown in Figure 2a are paired [$CO_2$] and $\delta^{13}C$ data along with the best-fit Model I ordinary least squares (OLS) isotopic mixing line for a typical night. Data from all measurement inlets between the hours of 9 PM and 3 AM local time were used to generate this isotopic mixing line. In this example, $\delta_R$ and $\phi$ can be adequately constrained from the data as evidenced by the high $r^2$ value of 0.99, the low uncertainties for $\delta_R$ and $\phi$ (0.3‰ and 152‰ ppm) respectively, and the large [$CO_2$] range for the mixing line (52 ppm). We typically found high [$CO_2$] ranges most nights during the study period. Large [$CO_2$] ranges reduce the variability and the uncertainty in the estimate of $\delta_R$ [*Pataki et al.*, 2003; *Zobitz et al.*, 2006].

[27] The eddy isoflux, $F_{eddy-isoflux}$, is a key parameter in equations (2) and (4). This cannot at present be measured directly as $F_{eddy}$ with eddy covariance, however $F_{eddy-isoflux}$ is approximately equal to $\delta_N F_{eddy}$, where $\delta_N$ is a the intercept of a daytime Keeling plot through the roughness sublayer above the canopy [*Ogée et al.*, 2003b]:

$$\delta_a = c_B \frac{(\delta_B - \delta_N)}{c_a} + \delta_N = \frac{\beta}{c_a} + \delta_N \qquad \text{(day)}. \tag{6}$$

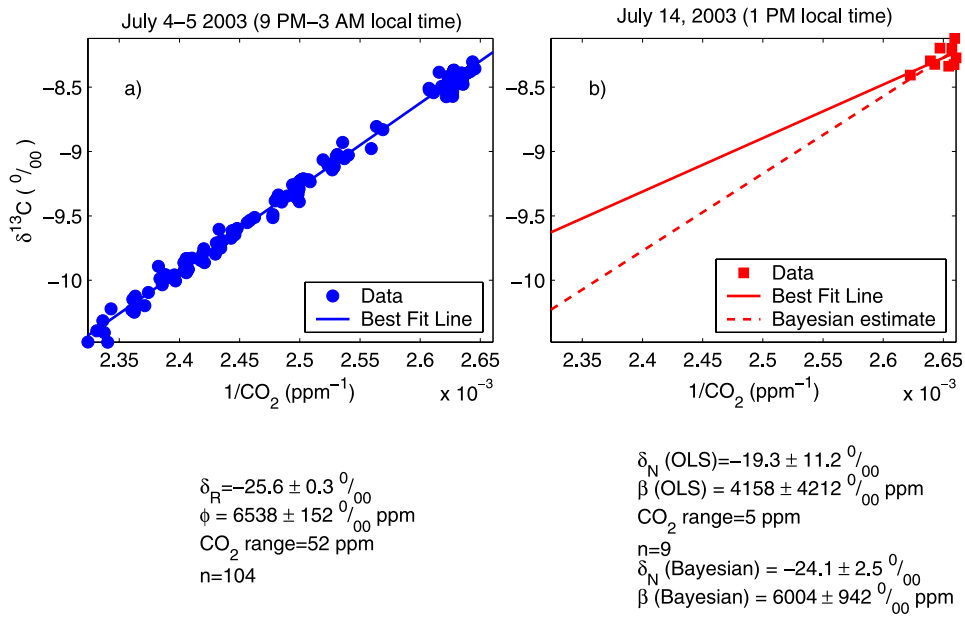


**Figure 2.** Typical isotopic mixing lines found during the study period. (a) Typical nighttime isotopic mixing line (Keeling plot) to estimate $\delta_R$ and $\phi$. The solid line was generated using the ordinary least squares estimate of the mixing line intercept ($\delta_R$) and slope ($\phi$). (b) Typical daytime isotopic mixing line (Keeling plot) to estimate $\delta_N$ and $\beta$. The solid line was generated using the ordinary least squares estimate of the mixing line intercept ($\delta_N$) and slope ($\beta$). The dashed line was generated using the Bayesian parameter estimate of $\delta_N$ and $\beta$.

In equation (6), $\beta$ (‰ ppm) is the slope of a daytime Keeling plot.

[28] As emphasized by *Ogée et al.* [2004], $\delta_N$ should be determined from measurements made above the roughness sublayer to avoid bias from concentration plumes from individual forest elements. For this study, the only measurement of $[CO_2]$ and $\delta^{13}C$ that best satisfied this requirement was at 21.5 m ($F$ measurement height). Low $[CO_2]$ ranges were common during the day, even when all measurement inlets were included. A typical isotopic mixing line for $\delta_N$ is shown in Figure 2b. Data used to determine $\delta_N$ come from all measurement inlets for a given half hour, hence there are only nine data points in Figure 2b. The OLS estimate of $\delta_N$ is quite uncertain, as evidenced by the large uncertainties on $\delta_N$ and $\beta$ and the low $[CO_2]$ range for the mixing line (5 ppm). These low $[CO_2]$ ranges lead to highly variable estimates of $\delta_N$ with large uncertainties [*Bowling et al.*, 2005; *Zobitz et al.*, 2006]. If we were to determine $\delta_N$ from only the 21.5 m inlet, isotopic mixing lines would be poorly constrained, therefore $\delta_N$ and $\beta$ were determined with measurements from all heights. However, determining $\delta_N$ from all inlets may bias the estimate from inlets near the ground. For these reasons, $\delta_N$ and $\beta$ are Bayesian-estimated parameters in this study.

[29] $F_A$ is related to the $CO_2$ mixing ratio in the chloroplast ($c_c$) via a standard conductance relationship:

$$F_A = \overline{g}(c_c - \overline{c}_a) \tag{7}$$

$$\frac{1}{\overline{g}} = \frac{1}{g_a} + \frac{1}{g_s} + \frac{1}{g_m}, \tag{8}$$

where $\overline{c}_a$ is the mean canopy $CO_2$ mixing ratio, and the overall conductance ($\overline{g}$) is composed of an aerodynamic conductance ($g_a$), surface conductance ($g_s$), and mesophyll conductance ($g_m$) (all conductance units mol $m^{-2}$ $s^{-1}$) [*Ogée et al.*, 2003b; *Knohl and Buchmann*, 2005]. The aerodynamic conductance is calculated in the same manner as *Ogée et al.* [2003b] (see equation (11) in *Ogée et al.* [2003b]) and *Knohl and Buchmann* [2005]. The surface conductance is obtained by inversion of the Penman-Monteith equation [*Grace et al.*, 1995] (see equation (9) in *Ogée et al.* [2003b]), and the mesophyll conductance was estimated for the conifers in this study to be 0.125 mol $m^{-2}$ $s^{-1}$ (W. K. Smith, personal communication).

[30] The parameter $\Delta_{canopy}$ represents the flux-weighted photosynthetic discrimination of the entire forest. This parameter expresses the fractionation of $^{13}CO_2$ when $CO_2$ is (a) transported through the leaf boundary layer, (b) diffuses into the stomatal cavity, (c) enters solution, (d) diffuses through the mesophyll to the sites of carboxylation, and (e) is reduced via photosynthesis. The total fractionation is given by equations (9) and (10) [*Vogel*, 1980; *Farquhar et al.*, 1989; *Farquhar and Lloyd*, 1993]:

$$\Delta_{canopy} = \overline{a} + (b_R - \overline{a})\frac{c_c}{\overline{c}_a} \tag{9}$$

$$\overline{a} = \frac{a_b g_s g_m + a g_a g_m + (a_s(T) + a_1) g_s g_a}{g_s g_m + g_a g_m + g_s g_a}, \tag{10}$$

where $b_R$ is the enzymatic fractionation of carbon reduction (≈27.5‰), $a_b$ is the leaf boundary layer fractionation (2.9‰), $a$ is the fractionation due to molecular diffusion

across the stomata (4.4‰), $a_s(T)$ the temperature-dependent fractionation as $CO_2$ enters solution (assumed constant at 1.1‰ at 25°C), and $a_1$ the fractionation due to diffusion within the mesophyll (0.7‰).

### 3.2. Environmental Regression Methods

[31] Environmental regression methods consist of flux partitioning techniques that directly utilize measurements such as incoming radiation ($Q_P$) or air temperature ($T$) to partition $F$ into *GEE* and *TER*. For this study, two different environmental regression methods were utilized. The fundamental difference between the methods utilized is the prescribed dependency of *GEE* and *TER* on environmental drivers $Q_P$ and $T$.

[32] Temperature-based statistical flux partitioning: A review of temperature-based partitioning methods was provided by *Reichstein et al.* [2005a]. Temperature-based statistical flux partitioning was carried out using the method exactly detailed in *Reichstein et al.* [2005a]. We briefly describe the relevant parts of the theory here. Estimates of *GEE* and *TER* from this method are referred to as "statistical flux partitioning." At night, $GEE = 0$, implying $F = TER$. Nighttime regressions of $F$ and air temperature ($T$) are calculated using an exponential regression model [*Lloyd and Taylor*, 1994]:

$$TER = R_{ref} \exp\left[E_0\left(\frac{1}{T_{ref} - T_0} - \frac{1}{T - T_0}\right)\right], \tag{11}$$

where $T_0 = -46$°C, $T_{ref} = 10$°C. The temperature independent respiration rate ($R_{ref}$) and temperature sensitivity ($E_0$) were free parameters. The temperature sensitivity $E_0$ is estimated through least squares regression on a 15-day timescale, but then averaged and assumed to be constant in time. Then a temporally-varying estimate of $R_{ref}$ is generated through least squares estimation, hence linking variation in $F$ between shorter and longer timescales. Once $R_{ref}(t)$ and $E_0$ (constant) are determined, daytime *TER* is modeled with equation (11) from measured air temperature, and *GEE* is estimated as the difference between $F$ and *TER*. The estimated values of $R_{ref}(t)$ and $E_0$ with their standard errors are utilized to generate different *TER* estimates and subsequently an estimate of the intrinsic uncertainty in a *TER* estimate. When this was done, *TER* uncertainty was conservatively estimated to be 3 $\mu$mol m$^{-2}$ s$^{-1}$.

[33] Nonparametric flux partitioning: A second method to estimate *GEE* and *TER* from $F$ is to use nonparametric regression as described in *Yi et al.* [2004]. For this flux partitioning routine, *TER* is assumed to be exponentially related to daytime air temperature ($T$) and *GEE* is assumed to be a saturating function of photosynthetically active radiation ($Q_P$):

$$F = GEE + TER \tag{12}$$

$$= \frac{\alpha_1(T) Q_P \alpha_2(T)}{\alpha_1(T) Q_P + \alpha_2(T)} + TER(T) \tag{13}$$

[34] The parameters $\alpha_i(T)$ that characterize the functional relationship for *GEE* are assumed to be dependent on temperature. The functional parameters for $\alpha_i(T)$ and parameters characterizing the *TER*-air temperature relationship are determined with $F$, air temperature, and $Q_P$ data and then minimizing the difference between measured $F$ and the sum of functional forms of *GEE* and *TER* (equation (13)) using nonlinear weighted least squares. Estimates of *GEE* and *TER* from this method are referred to as "nonparametric flux partitioning."

### 3.3. Bayesian Parameter Estimation

[35] All the flux partitioning methods described in section 3.1 have a model that relates data (e.g., $F$) to parameters (e.g., $F_A$ and $F_R$ or *GEE* and *TER*). However the parameter estimation technique utilized can vary, as evidenced by the two different flux partitioning methods described in section 3.2. More generally, the goal of any parameter estimation technique is to estimate parameters $\vec{m}$ from data $\vec{d}$ by assuming a model $G$ (where $G$ is either linear or nonlinear) between parameters and data ($G(\vec{m}) = \vec{d}$).

[36] Bayesian parameter estimation is a statistical technique that estimates $\vec{m}$ from $\vec{d}$ and also uses prior information about $\vec{m}$ in the estimation routine. Introductions to Bayesian parameter estimation techniques can be found in *Tarantola* [2005] and *Gubbins* [2004]. Data and prior parameter distributions are inputs into Bayes theorem, which is used to generate a posterior probability density function of estimated parameters, conditional on data and prior parameter values and their respective uncertainties [*Jaynes*, 2003; *Tarantola*, 2005]. The first two moments of this posterior probability density function (mean and variance) can be used to characterize the posterior results and uncertainty. The conditionality of the Bayesian parameter estimate on data and prior parameter distributions differs from traditional parameter estimation techniques.

[37] The process model $G$ relating $\vec{m}$ to parameters $\vec{d}$ used to determine a Bayesian isotope flux partitioning consists of equations (3), (4), (6), (7), and (9). Equations (3), (4), (7), and (9) define a system of four equations for the four unknowns $F_A$, $F_R$, $\Delta_{canopy}$, and $c_c$. However, equation (9) can be solved for $c_c$ and combined with equation (7). As a result, we have the following system of equations with unknowns $F_A$, $F_R$, and $\Delta_{canopy}$, $\delta_N$, and $\beta$:

$$\begin{aligned}
F_A + F_R &= F \\
\left(\overline{\delta}_a - \Delta_{canopy}\right) F_A + \delta_R F_R &= \delta_N F_{eddy} + F_{isostorage} \\
-F_A + \Delta_{canopy} \frac{\overline{c}_a \overline{g}}{b_R - \overline{a}} &= \frac{\overline{c}_a \overline{g} b_R}{b_R - \overline{a}} \\
\frac{\beta}{c_a^1} + \delta_N &= \delta_a^1 \\
\vdots \qquad & \qquad \vdots \\
\frac{\beta}{c_a^i} + \delta_N &= \delta_a^i \\
\vdots \qquad & \qquad \vdots \\
\frac{\beta}{c_a^9} + \delta_N &= \delta_a^9,
\end{aligned} \tag{14}$$

where $c_a^i$ and $\delta_a^i$ represent a measurement of $[CO_2]$ and $\delta^{13}C$ made at a particular measurement location (height above

**Table 2.** Entries of $\vec{d}$ With the Percentage That Observed Quantity Was Available[a]

| Observed Quantity | Measurement Standard Deviation | Percent Coverage |
|---|---|---|
| $F$ ($\mu$mol m$^{-2}$ s$^{-1}$) | 2[b] | 64% |
| $F_{isostorage}$ ($\mu$mol ‰ m$^{-2}$ s$^{-1}$) | 50 | 76% |
| $\frac{\overline{c}_a \overline{g} b_R}{b_R - \overline{a}}$ ($\mu$mol m$^{-2}$ s$^{-1}$) | 2 | 57% |
| $\delta_a$ (‰) | 0.15 | 57% |

[a]Percent coverage values are out of 2734 possible half-hourly observations. The square of the sample standard deviation is the corresponding diagonal entry in $C_D$.

[b]The standard deviation of $F$ is linearly scaled with $u*$ as done in *Ogée et al.* [2004] from a value of 2 at $u_* = 0.3$ $m$ $s^{-1}$ to a value of 6 $\mu$mol m$^{-2}$ s$^{-1}$ at $u_* = 0.6$.

ground) where $i$ = 1 (0.1 m), 2 (0.5 m),..., 9 (21.5 m). Equation (14) is the process model used in the Bayesian parameter estimation routine and consists of 12 equations for 5 unknowns. As a result, for each half-hourly estimate, the vector $\vec{m}$ of estimated parameters is:

$$\vec{m} = \left[F_A \; F_R \; \Delta_{canopy} \; \delta_N \; \beta\right]^T, \tag{15}$$

where $(\,)^T$ denotes the transpose operation. The data vector $\vec{d}$ consists of:

$$\vec{d} = \left[F \; F_{isostorage} \; \frac{\overline{c}_a \overline{g} \; b_R}{b_R - \overline{a}} \; \delta_a^1 \; ... \; \delta_a^i \; ... \; \delta_a^9\right]^T. \tag{16}$$

[38] To determine a Bayesian parameter estimate $\vec{m}*$ for the linear problem ($G(\vec{m}) = G\vec{m}$, where $G$ is now a matrix) three assumptions are made. First, we assume that the observations $\vec{d}$ arise from a multivariate normal distribution with mean $G\vec{m}$ and covariance matrix $C_D$. The second assumption is that measurements are independent and uncorrelated. The combination of the first two assumptions prescribes $C_D$ to be a diagonal matrix containing the square of the standard deviation of a particular measurement. Values of $C_D$ for this study are reported in Table 2. The third assumption is that the prior distribution for parameters $\vec{m}$ is multivariate normal with mean $\vec{m}_{prior}$ and covariance matrix $C_M$. The matrix $C_M$ is a diagonal matrix as well, where the diagonal entries contains the square of the standard deviation of a particular parameter. We discuss values of $\vec{m}_{prior}$ and $C_M$ below. With these three assumptions, it can be shown that the posterior distribution of $\vec{m}*$ is normal as well [*Tarantola*, 2005]. As a result, the first two moments of this distribution (mean and square of the standard deviation) characterize the posterior distribution of $\vec{m}$ and are given by equations (17) and (18):

$$\vec{m}* = \vec{m}_{prior} + C_M G^T \left(G C_M G^T + C_D\right)^{-1} \left(\vec{d} - G\vec{m}_{prior}\right) \tag{17}$$

$$\tilde{C}_M = \left(G^T C_D^{-1} G + C_M^{-1}\right)^{-1}, \tag{18}$$

where $\vec{m}$, $\vec{d}$, and $G$ are defined above and $(\,)^{-1}$ denotes the inverse operation. In equation (17), $\vec{m}*$ is the mean value of the posterior distribution for $\vec{m}$. In equation (18), $\tilde{C}_M$ is the posterior covariance matrix for $\vec{m}$. The square root of the diagonal of $\tilde{C}_M$ contains the posterior standard deviations of $\vec{m}$. For a nonlinear problem (i.e., $G(\vec{m}) \neq G\vec{m}$), the solution for $\vec{m}*$ is found by numerical methods [*Tarantola*, 2005]. Some measurements (such as $F_{eddy}$, $\overline{\delta}_a$, $\overline{c}_a$, $c_a^i$) or experimentally-derived parameters (such as $\delta_R$, $\overline{g}$, $b_R$, $\overline{a}$) may have their own appreciable uncertainties. For this study we make the assumption that the uncertainty in these quantities does not unduly influence the Bayesian parameter estimate of $\vec{m}$.

[39] The agreement between $G(\vec{m}*)$ and $\vec{d}$ will depend on the values of $\vec{m}_{prior}$ and $C_M$. Because of this $\vec{m}*$ may not be exactly equal to a least squares estimate of $\vec{m}$. As a result, equation (17) may be biased towards $\vec{m}_{prior}$. For example, this bias can result if a prior mean value of $F_R$ is 20 $\mu$mol m$^{-2}$ s$^{-1}$, and the posterior Bayesian parameter estimate is 18 $\mu$mol m$^{-2}$ s$^{-1}$, but a statistical flux partitioning estimate of $F_R$ yields 5 $\mu$mol m$^{-2}$ s$^{-1}$. This sensitivity could arise from two factors: lack of linear independence in the process model $G$ or weighting $\vec{m}_{prior}$ too strongly by having small variance estimates in $C_M$. If there is a lack of linear independence, using a Bayesian approach in this case specifies additional constraints (the prior values) so that the system automatically becomes well-posed [*Gubbins*, 2004], leading to a unique solution. If the prior variance estimates are too small, then it can be shown that in the limit as the prior variances approach zero, equation (17) reduces to $\vec{m}_{prior}$.

[40] The posterior correlation matrix $E$ is a tool that can help ascertain if two parameters have been independently resolved by the data set [*Tarantola*, 2005]. Denote the element $ij$ of $\tilde{C}_M$ by $\tilde{C}_M^{ij}$, and element the $ij$ of $E$ in a similar manner. Then entries of the posterior correlation matrix are:

$$E^{ij} = \frac{\tilde{C}_M^{ij}}{\sqrt{\tilde{C}_M^{ii}}\sqrt{\tilde{C}_M^{ij}}}. \tag{19}$$

It can be shown that entries of $E$ vary between $-1$ and 1 [*Tarantola*, 2005]. In a non-Bayesian context, $E$ represents the correlation between two estimated parameters. In the Bayesian context this is still true, however a strong correlation (or anticorrelation) on off-diagonal entries of $E$ indicates that the data set cannot independently resolve the two parameters but rather some combination of the parameters. Hence the model is poorly parameterized and additional constraints (such as prior information) is needed to resolve these parameters [*Tarantola*, 2005].

**Table 3.** Prior Mean and Standard Deviation for Each of the Prior Parameter Distributions Used in the Study Assuming the Probability Distribution of These Parameters is Normal[a]

| Parameter | Prior Mean | Prior Standard Deviation |
|---|---|---|
| $F_A$ ($\mu$mol m$^{-2}$ s$^{-1}$) | $-10$ | 10 |
| $F_R$ ($\mu$mol m$^{-2}$ s$^{-1}$) | 5; $F_R(T)$[b] | 5; 3 |
| $\Delta_{canopy}$ (‰) | 17 | 10 |
| $\delta_N$ (‰) | $-24.5$ | 10 |
| $\beta$ (‰ ppm) | 6100 | 1000 |

[a]The prior means are entries of $\vec{m}_{prior}$ and the square of the standard deviation is the corresponding diagonal entry of $C_M$.

[b]The prior mean and standard deviation was specified from nighttime $F$ and statistical temperature regressions, following *Reichstein et al.* [2005a]. See discussion in the text for how the standard deviation was selected.

[41] For this study Bayesian parameter estimates of $\vec{m}$ were derived using two different sets of prior mean values and standard deviations for certain parameters. These scenarios are the following and are summarized in Table 3.

[42] Fixed-in-time priors: Prior mean values and their respective standard deviations are fixed in time for each half-hourly measurement period, as done in *Ogée et al.* [2004]. Prior values and standard deviations of $F_A$ are $-10 \pm 5$ $\mu$mol m$^{-2}$ s$^{-1}$, $F_R = 5 \pm 5$ $\mu$mol m$^{-2}$ s$^{-1}$. The standard deviations for $F_A$ and $F_R$ are similar to those used in *Ogée et al.* [2004]. Additional prior mean values and standard deviations are $\Delta_{canopy} = 17 \pm 10$‰, $\delta_N = -24.5 \pm 10$‰, and $\beta = 6100 \pm 1000$‰ ppm. The prior mean values for $\delta_N$ and $\beta$ are derived from a Keeling-plot regression using all daytime [$CO_2$] and $\delta^{13}C$ data at 21.5 m over the measurement period.

[43] Temperature-based priors: In this case, the prior mean value for $F_R$ was set equal to the estimated daytime *TER* using the statistical flux partitioning routine described in section 3.2, herein referred to as ''T-based priors.'' The standard deviation for $F_R$ is fixed-in-time at 3 $\mu$mol m$^{-2}$ s$^{-1}$, as described in section 3.2. All the other prior parameter values ($F_A$, $\Delta_{canopy}$, $\delta_N$, $\beta$) are the same as fixed-in-time priors. Estimates of *TER* from the nonparametric flux partitioning routine were not used as a prior mean value for $F_R$.

[44] Each of these scenarios are used to generate Bayesian parameter estimates of $\vec{m}$ at half-hourly timescales. As a result, two sets of posterior parameter mean values and standard deviations were generated: (a) half-hourly estimates derived from fixed-in-time prior values, (b) half-hourly estimates derived from T-based prior values. We also ran an additional Bayesian parameter estimation routine at daily time steps from 9 AM-3 PM local time, representing an aggregated midday estimate of $\vec{m}$. Since the conclusions from the daily Bayesian parameter estimates did not differ from those based on the half-hourly estimates, these results are not discussed.

### 3.4. A New Application of Bayes' Theorem to *F* Partitioning

[45] There are three important differences between this study and that of *Ogée et al.* [2004]. First, there are orders of magnitude more measurements of [$CO_2$] and $\delta^{13}C$ measurements available for this study than *Ogée et al.* [2004]. That study used flask-collected data collected over a single diurnal period. In contrast, for this study the [$CO_2$] and $\delta^{13}C$ data collected by TDL spectroscopy spans 104 days. This high-resolution data led to 942 time periods that were isotope flux-partitioned that span a wide range of meteorological conditions. This data density allows for examination of both diurnal patterns of $F_A$ and $F_R$ as well as bin-averaged diurnal patterns over the study period.

[46] Second, the process model used in the Bayesian parameter estimation differs from *Ogée et al.* [2004]. For that study, equations (1) and (2) only were used in the Bayesian parameter estimation. Here additional equations describing $\Delta_{canopy}$ are $\delta_N$ (see equation (14)) are included in the process model for Bayesian parameter estimation.

[47] Third, the high-density data set allowed further determination of $\delta_N$ than what was done in *Ogée et al.* [2004]. In particular, *Ogée et al.* [2004] held the value of $\delta_N$ constant over the diurnal pattern. For this study, $\delta_N$ is Bayesian-estimated parameter determined every half-hour from a Keeling-plot regression of [$CO_2$] and $\delta^{13}C$ using all sampling heights measured.

## 4. Results

[48] Our first objective was to generate Bayesian parameter estimates of $F_A$, $F_R$, $\Delta_{canopy}$, $\delta_N$, and $\beta$. At each time step, the posterior correlation matrix $E$ was also calculated. In general, the posterior standard deviation of all the parameters was reduced from the prior standard deviation (results not shown), indicating that the data indeed contained information that reduced the prior uncertainty of the parameters.

[49] Figure 3 shows a subset of the partitioned data using both non-Bayesian (Figures 3c and 3d) and Bayesian (Figure 3e) techniques to determine flux partitioning estimates. Overall a diurnal pattern in both posterior mean estimates of $F_A$ and $F_R$ using either fixed-in-time or T-based priors was produced. This is in agreement with other diurnal patterns generated from isotope flux partitioning [*Bowling et al.*, 2001; *Ogée et al.*, 2003b; *Knohl and Buchmann*, 2005]. A similar diurnal pattern for non-Bayesian statistical flux partitioning of $F$ into *GEE* and *TER* was generated (Figure 3c). Figure 3d presents isotope flux partitioning estimates generated without Bayesian parameter estimation following the solution given in the Appendix of *Bowling et al.* [2001]. Examining Figure 3a with Figures 3c–3e suggests that $F_A$ (or *GEE*) has a diurnal pattern that correlates with diurnal trends of photosynthetically active radiation ($Q_P$), with $F_A$ (*GEE*) increasing from zero to a midday maximum at noon.

[50] Figure 4 shows Bayesian values of $F_A$ and $F_R$ or *GEE* and *TER* in the context of expected canopy biophysical relationships. Half-hourly estimates of $F_A$ and $F_R$ are grouped in incremental bins of photosynthetically active radiation ($Q_P$) or air temperature and the mean value and standard deviation of each bin are shown. Figure 4a shows the binned data of $Q_P$ versus $F_A$. Figure 4c shows the binned data of air temperature versus $F_R$. In addition, Figures 4a and 4c show the response of prior mean values of $F_A$ and $F_R$ to $Q_P$ and air temperature respectively. These values were binned because examination of the half-hourly data suggested a meaningful trend in the raw data (results not shown), however this trend was masked due to measurement stochasticity over the long time period (3 months). Binning the results in this manner allows one to see the underlying relationship in the fluxes [e.g., *Greco and Baldocchi*, 1996]. Clearly, posterior estimates of $F_A$ and $F_R$ generated from fixed-in-time priors were higher than posterior estimates from T-based priors. Posterior estimates of $F_A$ generated from both fixed-in-time and T-based priors produced a saturating light response curve of $F_A$ (Figure 4a). However, Bayesian estimates of $F_R$ from fixed-in-time priors show no relationship with temperature, and the temperature sensitivity of posterior estimates of $F_R$ from T-based priors strongly matches prior parameter temperature sensitivity (Figure 4c). For comparison, Figures 4b and 4d show the $Q_P$ or temperature response curve for $F$ from *Yi et al.* [2004].

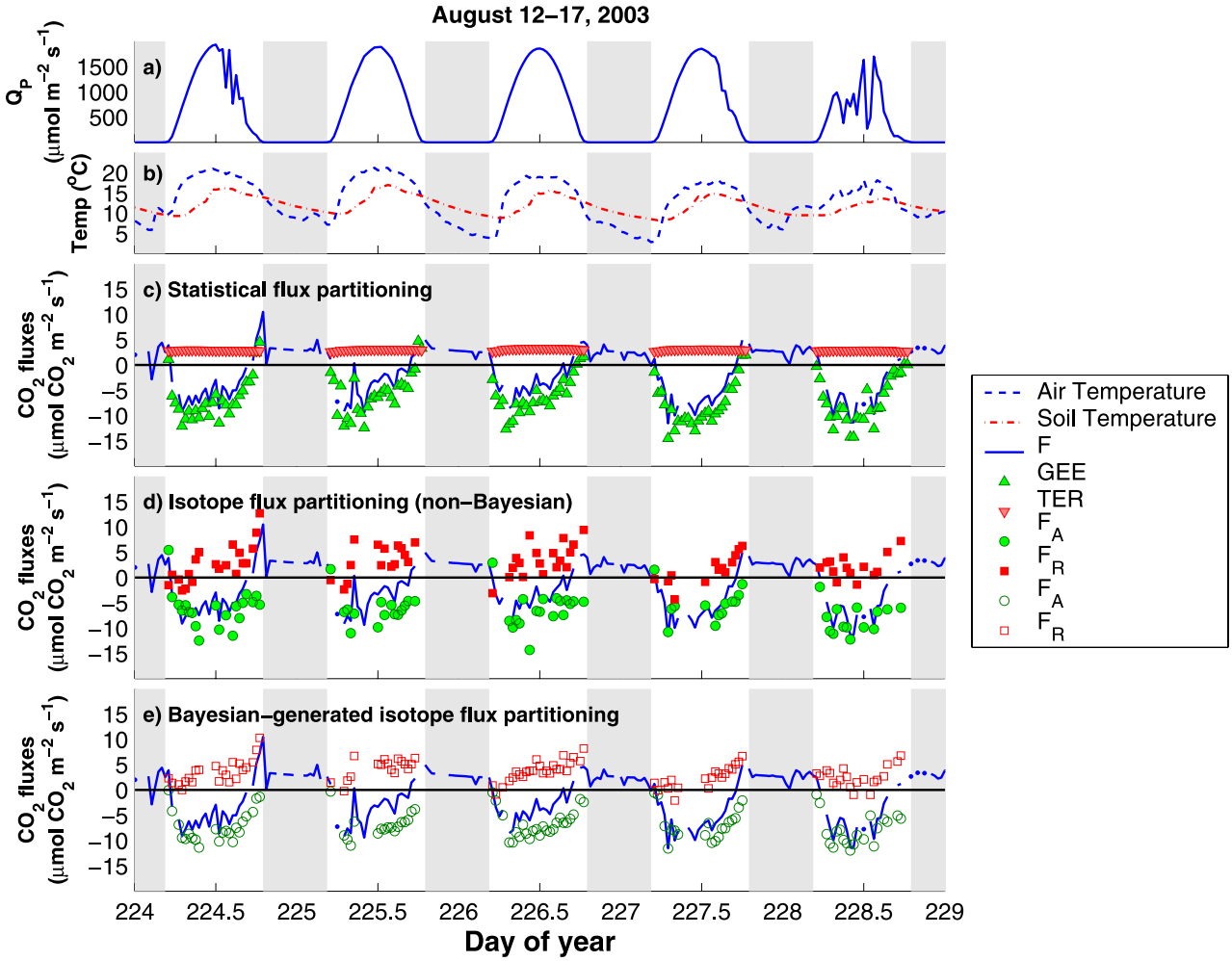


**Figure 3.** Half-hourly partitioning results and associated environmental variables from August 12–17, 2003. Nighttime periods are indicated with grey shading. (a) Photosynthetically active radiation ($Q_P$), (b) air temperature (dashed line) and soil temperature (dash-dot line), (c) non-Bayesian statistical flux partitioning of *GEE* and *TER*, and (d) non-Bayesian isotope flux partitioning of $F_A$ and $F_R$. (e) $F_A$ and $F_R$ obtained from Bayesian parameter estimation using fixed-in-time priors. Similar results for T-based priors were obtained and hence not shown.

[51] Figures 3 and 4 suggest that the estimates of $F_A$ and $F_R$ from the Bayesian parameter estimation routine are dependent on the choice of prior parameters for $F_A$ and $F_R$. Consequently the data may not be able to independently resolve these parameters. This is confirmed by examining the posterior correlation matrix $E$. Taken as an ensemble average of the entire sampling period, a graphical representation of $E$ for posterior parameter estimates generated from fixed-in-time prior values is shown in Figure 5. As the covariance matrix was symmetric, only lower diagonal entries of $E$ are shown. Similar results for $E$ using T-based prior values were obtained and hence are not shown. Figure 5 is structured so that the vertical axis of each subplot represents the correlation of a posterior parameters uncertainty to the parameters in the title of the top row. The horizontal axis represents a particular time of day. If the posterior parameter correlation between two different parameters is zero, this implies the data set can adequately resolve the two parameters. If this is not the case, some linear combination of the parameters is resolved by the data [*Tarantola*, 2005]. Hence prior parameter values or additional data related to the processes (or parameters) of interest are needed to independently resolve the two parameters. Figure 5 shows that $\Delta_{canopy}$ is positively correlated with $F_A$, but also negatively correlated with $F_R$. Hence more informative priors or additional data for $\Delta_{canopy}$ would be helpful in resolving this parameter.

[52] Figure 6 shows how the sum of *GEE* and *TER* (Figure 6a) from statistical flux partitioning or Bayesian-estimated $F_A$ and $F_R$ (Figure 6b) compare to measured $F$. Figure 6c compares measured $F_\delta$ to estimated $F_\delta$ from the left hand side of equation (2) using Bayesian estimated parameters. Values of $\delta_N$ for the measured $F_\delta$ were derived from OLS regression using equation (6). In Figure 6 the Bayesian estimated parameters were derived from fixed-in-time prior values. Similar results for T-based priors were derived and hence not shown.

[53] Shown in Figure 7 are the diurnal ensemble averages of posterior parameter estimates of $F_A$, $F_R$, $\Delta_{canopy}$ and $\delta_N$ from fixed-in-time priors (empty symbols) and temperature

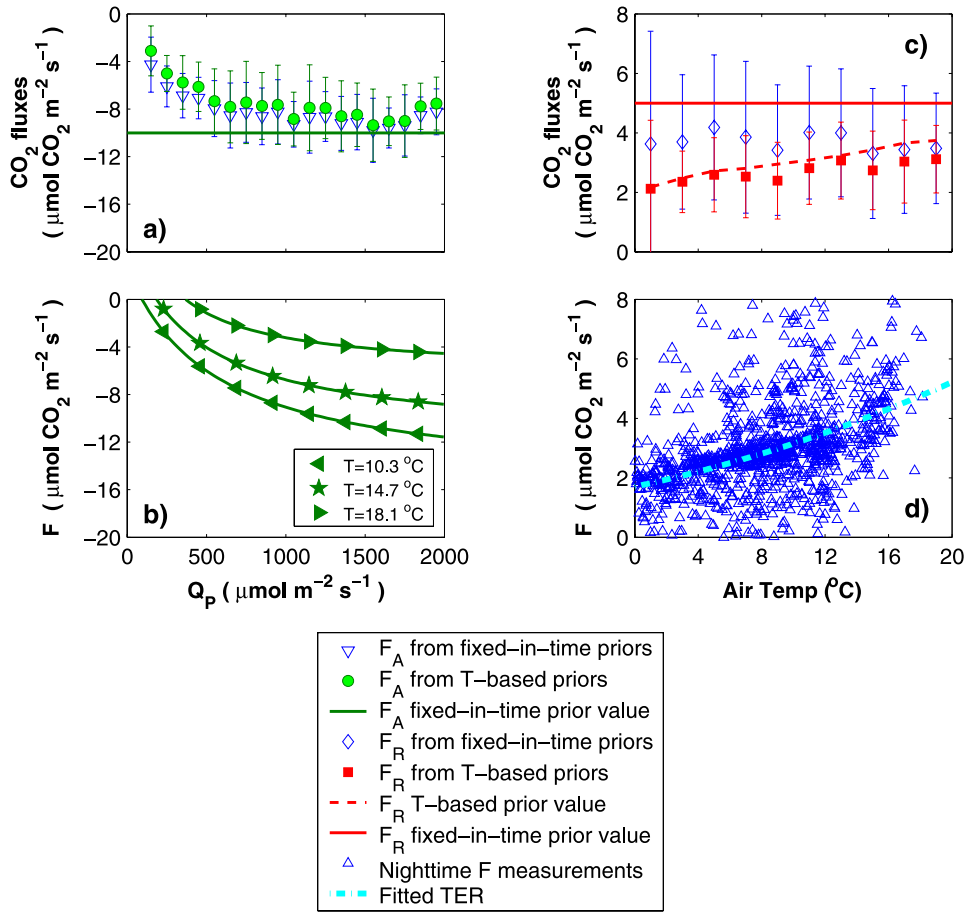


**Figure 4.** Regression of posterior Bayesian parameter estimates $F_A$ and $F_R$ against photosynthetically active radiation ($Q_P$) and air temperature respectively. (a and c) Binned data of posterior estimates of $F_A$ ($F_R$) either from fixed-in-time prior values (triangles or diamonds) or temperature based priors (circles or squares), along with the binned response curves of the fixed-in-time prior values (solid line) and T-based priors (dashed line). Periods with $Q_P$ less than 100 $\mu$mol m$^{-2}$ s$^{-1}$ were excluded from the averaging. $Q_P$ was binned in 100 $\mu$mol m$^{-2}$ s$^{-1}$ increments, and air temperature was binned in 2 C increments. (b) Light response curves of $F$ for fixed values of temperature at Niwot Ridge from *Yi et al.* [2004], and (d) nighttime $F$ measurements versus air temperature for the 2003 sampling period along with the temperature response curve for *TER* at Niwot Ridge from *Yi et al.* [2004].

based priors (solid symbols), along with measured $\delta_R$ and the calculated isotopic disequilibrium ($\mathcal{D} = \delta_A - \delta_R$). Posterior estimates generated by both fixed-in-time and T-based priors suggest that $\delta_A > \delta_R$ or $\mathcal{D} > 0$ at midday. The prior isotopic disequilibrium was 0‰, generated from the prior values of $\Delta_{canopy}$ = 17‰, and $\delta_R \approx -25$‰, with the average value of $\delta_A$ (−8‰).

## 5. Discussion

### 5.1. Bayesian Parameter Estimation on Half-Hourly Timescales

[54] One of the objectives of this study was to compare isotope-partitioned fluxes of $F_A$ and $F_R$ to expected canopy biophysical relationships. Figure 4a provides evidence that $F_A$ is indeed a saturating function of incoming radiation, even for posterior Bayesian estimates generated from either fixed-in-time or T-based prior values. However, posterior estimates of $F_R$ were only sensitive to temperature when T-based prior values were used (Figure 4c). This difference of the $F_R$ temperature sensitivity between fixed-in-time and T-based prior values may arise from two possibilities: (a) biological factors preventing the establishment of a robust $F_R$-temperature relationship, and (b) sensitivity of the Bayesian parameter estimation routine to prior parameter values.

[55] The temperature sensitivity of $F_R$ may not be as strong as expected compared to the *TER* temperature sensitivity. As discussed in section 1, scaling respiration with temperature may be confounded by other covariates such as moisture or substrate availability. The dynamic microbial community at Niwot Ridge also confounds such relationships [*Monson et al.*, 2006], as each community may have different temperature sensitivities on a seasonal timescale. While soil temperature may influence $F_R$ more than air temperature, using soil temperature did not lead to more robust functional relationships (results not shown). The other environmental regression flux partitioning routines in this study additionally use air temperature to determine

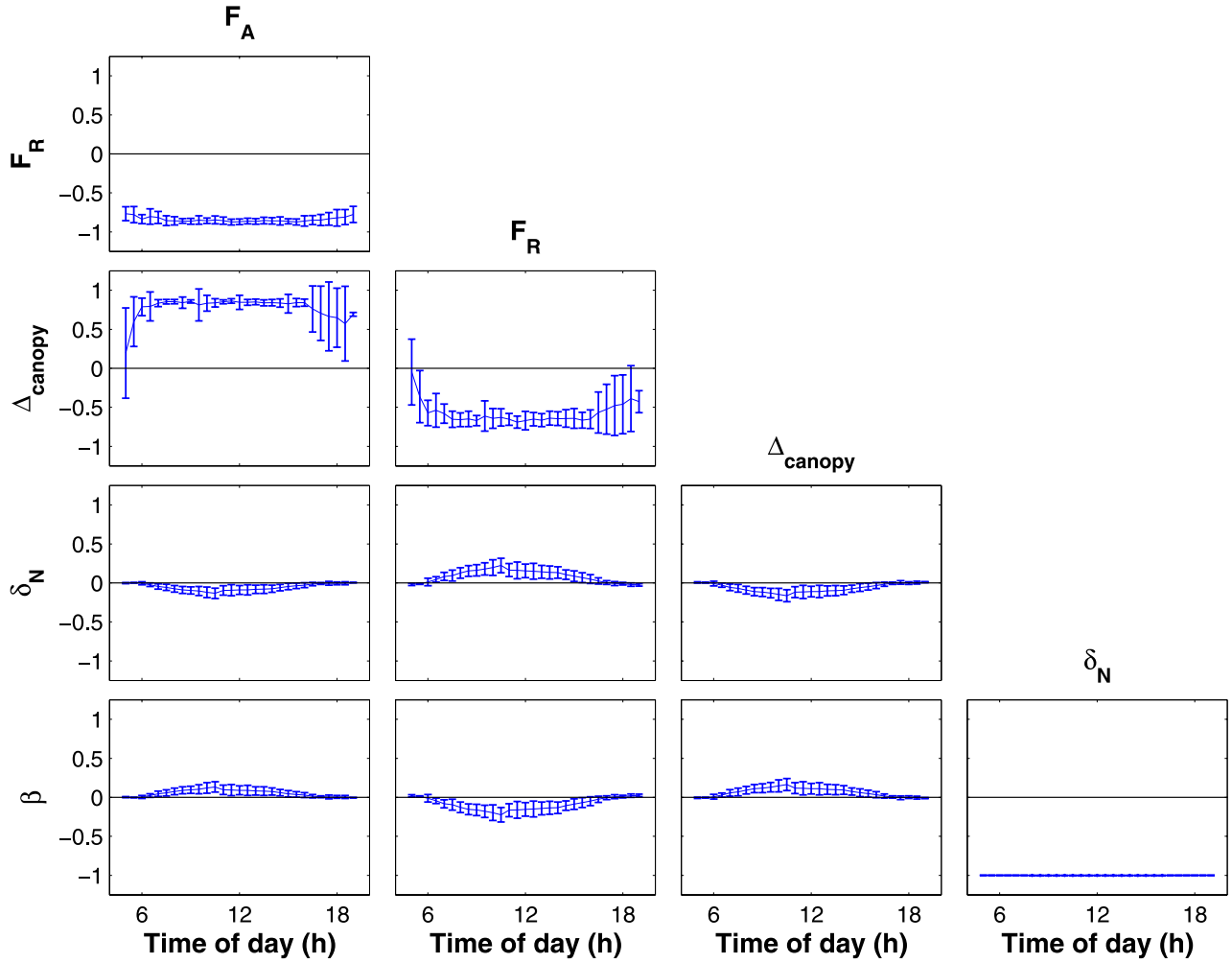


**Figure 5.** Lower triangular entries of the posterior correlation matrix derived from fixed-in-time prior values, taken as an ensemble average over the summer 2003 sampling period. See section 3.3 for a description of the posterior correlation matrix.

*TER*, hence for consistency, regressions with air temperature are presented in Figure 4c.

[56] Isotope partitioned $F_A$ matched other studies conducted at Niwot Ridge to a first approximation. From individual needle measurements for each of the dominant conifer species at the site, *Huxman et al.* [2003] found midsummer leaf-area based estimates of $F_A$ to be between $-2$ to $-5$ $\mu$mol m$^{-2}$ s$^{-1}$ at leaf temperatures of 10–20°C and saturating light, with variation in photosynthetic rates among each of the dominant species. When scaled with estimated LAI at Niwot Ridge (4.2 m$^2$ leaf area m$^{-2}$ ground area [*Monson et al.*, 2002]) these values range from $-8$ to $-20$ $\mu$mol m$^{-2}$ s$^{-1}$ for $F_A$. These estimates assume photosynthesis scales linearly with leaf area, however other factors (e.g., nonlinear light penetration through the canopy) may affect our simplistic scaling arguments [*Dang et al.*, 1997].

[57] For comparison, Figure 4b shows Niwot Ridge light response curves of $F$ and $Q_P$ from *Yi et al.* [2004] and Figure 4d shows nighttime measurements of $F$ and the Niwot Ridge temperature response curve of nighttime $F$ from *Yi et al.* [2004]. Our isotope-derived $F_A$ and $F_R$ fluxes are generally consistent with the independent methods of *Reichstein et al.* [2005a] and *Yi et al.* [2004] (Figure 4). However they appear to be particularly sensitive to the choice of prior values.

[58] The sensitivity to prior values can be explained by examining Figure 5. Note how Figure 5 has a decoupling of the correlations of the parameters $F_A$, $F_R$, and $\Delta_{canopy}$ from the parameters $\delta_N$ and $\beta$. This is most likely due to the fact that equation (14) is highly coupled in $F_A$, $F_R$, and $\Delta_{canopy}$, mildly so with $\delta_N$, and not at all with $\beta$. Figure 5 suggests that at a worst case scenario, the data can resolve $\delta_N$ and $\beta$ from $F_A$, $F_R$, and $\Delta_{canopy}$. The resolution of $\delta_N$ and $\beta$ from the other parameters most likely arises from the fact that at each half hour in the model for $G$, there are 9 separate equations (equation (6) at each measurement height) for these two parameters. The set of equations to determine $\delta_N$ and $\beta$ by itself is typically a well-posed and overdetermined mathematical system for $\delta_N$ and $\beta$. On the other hand we have exactly three equations (equation (14)) for the three parameters $F_A$, $F_R$, and $\Delta_{canopy}$.

[59] The sign of $\mathcal{D}$ is potentially very important for carbon cycle studies. *Randerson et al.* [2002] showed that

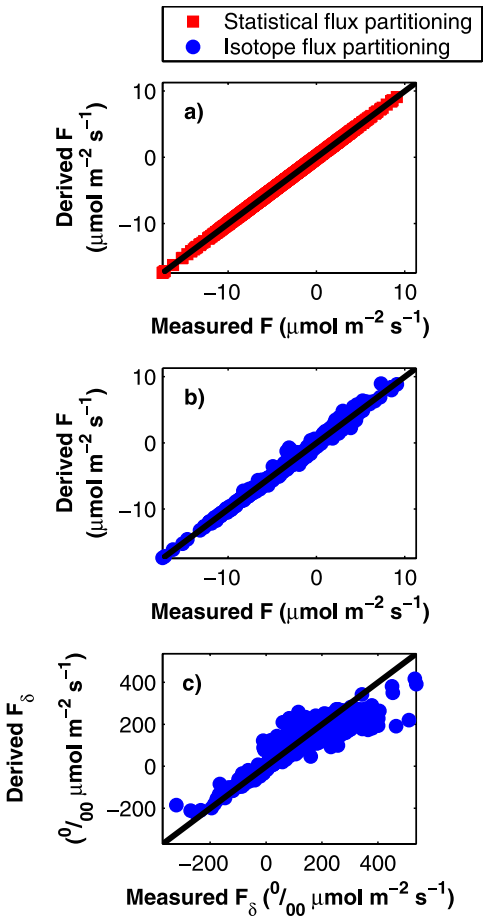


**Figure 6.** Comparison of measured and derived fluxes from Bayesian parameter estimation. (a) Comparison of measured $F$ to derived $F$ from statistical flux partitioning estimates of *GEE* and *TER*. The best fit line has slope 1.00, $r = 1$. (b) Comparison of measured $F$ to derived $F$ from Bayesian-generated isotope flux partitioning estimates derived with fixed-in-time prior values. The best fit line has slope 1.01, $r = 0.97$. (c) Comparison of measured $F_\delta$ to derived $F_\delta$ for Bayesian-generated isotope flux partitioning estimates derived with fixed-in-time prior values. The best fit line for has slope 0.80, $r = 0.94$. In all panels the 1:1 line is shown.

a 0.2‰ change in the global-scale analogy of $\Delta_{canopy}$ could alter the magnitude of the inferred terrestrial carbon sink by 25% (0.5 Pg C $yr^{-1}$), provided this 0.2‰ change was correlated with changes in *GEE*. Estimates of $\Delta_{canopy}$ from carbon cycle modeling studies at ecosystem, regional, or global scales generally have $\Delta_{canopy} = 17-19$‰ [*Ciais et al.*, 1995; *Randerson et al.*, 2002; *Baldocchi and Bowling*, 2003; *Scholze et al.*, 2003; *Suits et al.*, 2005], indicating for $C_3$ dominated systems that $\delta_A = \delta_A - \Delta_{canopy} \approx -8-18 = -24$ to $-26$‰, or that $\delta_A < \delta_R$ ($\mathcal{D} < 0$). Negative values of $\mathcal{D}$ are consistent with the widely-accepted concept of isotope disequilibrium between terrestrial photosynthesis and respiration. The $\delta^{13}C$ of atmospheric $CO_2$ has become more negative over the last two centuries due to the 13-C Suess effect [*Francey et al.*, 1999]. Since a large component of the respiratory flux consists of carbon that resides in the biosphere for many decades [e.g., *Trumbore*, 2000], $\delta^{13}C$ of the photosynthetic flux is expected to be more negative than the respiratory flux ($\mathcal{D} < 0$ [*Fung et al.*, 1997; *Yakir*, 2004]).

[60] In contrast, using the biophysical model ISOLSM to simulate carbon fluxes of $CO_2$ and $^{13}CO_2$ in a pine forest, *Aranibar et al.* [2006] found $\delta_A > \delta_R$. A study by *Tissue et al.* [2006] found leaf-level estimates of $\Delta$ to be 20‰ and values of $\delta_R = -26$‰. Given canopy $\delta^{13}C$ ratios are typically $-8$‰, this suggests for *Tissue et al.* [2006] study that $\delta_A - \Delta_{canopy} \approx -28$‰, indicating $\delta_A < \delta_R$. However, measurement-based isotope studies (including this study) frequently generate estimates of $\delta_A > \delta_R$ [*Bowling et al.*, 2001; *Miller et al.*, 2003; *Bowling et al.*, 2003a; *Ogée et al.*, 2003b; *Knohl and Buchmann*, 2005; *Lai et al.*, 2005; *Zhang et al.*, 2006]. With the data set used in the present study, *Bowling et al.* [2005] provided evidence for a consistent enrichment of canopy $\delta_R$ compared to ground $\delta_R$. If canopy $\delta_R$ reflects respiration of recent assimilation, and ground $\delta_R$ is more reflective of heterotrophic respiration, then this provides support for $\delta_A > \delta_R$. Furthermore, *Scartazza et al.* [2004] measured phloem sugars over the course of the growing season and consistently found these were more enriched than $\delta_R$. If the isotope ratio of phloem sugars reflects $\delta_A$, then this implies $\delta_A > \delta_R$. A sustained difference between $\delta_A$ and $\delta_R$ provides support for the hypothesis of post-photosynthetic fractionations [*Ghashghaie et al.*, 2003; *Tcherkez et al.*, 2003; *Badeck et al.*, 2005; *Tcherkez and Farquhar*, 2005; *Nogués et al.*, 2006]. We expect long-term (years to centuries) estimates of $\delta_A$ and $\delta_R$ to be the same because of mass conservation at the ecosystem scale. The possibility of unknown fractionations complicates this picture considerably.

[61] A common assumption of the isotopic method is that $\delta_R$ is constant during the day (we have made this assumption in the present study). This assumption may be incorrect. *Ogée et al.* [2004] discussed the appropriateness of using nighttime $\delta_R$ to estimate the isotopic signature of daytime nonfoliar respiration ($\delta_R$) and partially addressed this assumption by optimizing for $\delta_R$ in the study. However in *Ogée et al.* [2004] Bayesian parameter estimates of $\delta_R$ showed little diurnal variation (Figure 5 in *Ogée et al.* [2004]). In the absence of direct measurements of the isotopic signature of nonfoliar respiration, addressing the assumption that $\delta_R$ adequately represents the isotopic signature of daytime nonfoliar respiration is beyond the scope of the present study.

[62] As stated above, statistical flux partitioning produces estimates of *GEE* and *TER*, whereas the isotope method produces estimates of net photosynthetic uptake $F_A$ ($= GEE + F_L$) and nonfoliar respiration $F_R$ ($= TER - F_L$). As a result, temperature-based estimates are inappropriate for use as a prior for $F_R$ since foliar respiration is treated differently by the isotope [*Lloyd et al.*, 1996] or temperature-based [*Reichstein et al.*, 2005a] partitioning methods. However, as Figures 3 and 7 demonstrate, Bayesian parameter estimates from either fixed-in-time or T-based prior values yielded similar results within uncertainty.

[63] For this study, all the Bayesian parameter estimates cannot be independently resolved from the data (Figure 5). This implies that prior values for this application influence posterior parameter estimates. Yet if error bars were plotted in Figure 7, the results of $F_A$, $F_R$, $\Delta_{canopy}$, and $\mathcal{D}$ for either

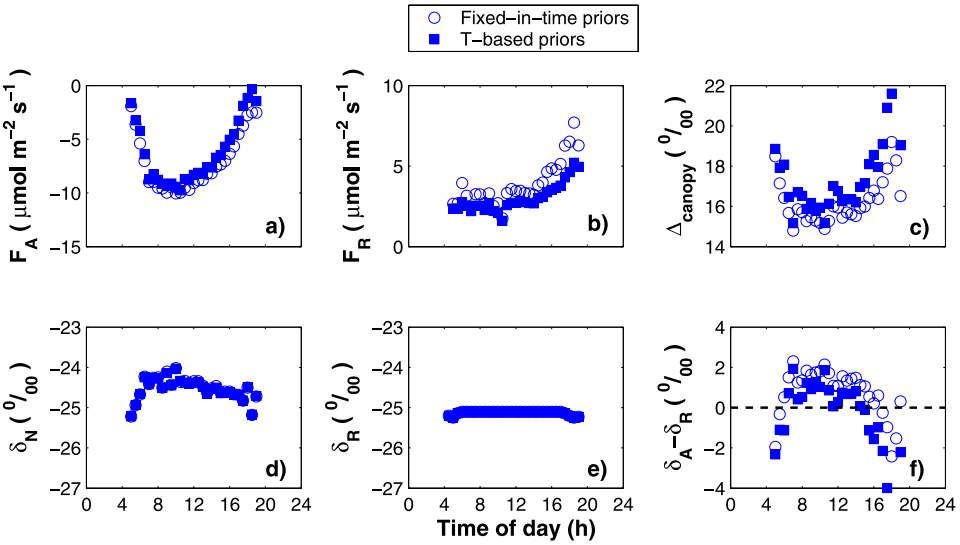


**Figure 7.** Comparison of diurnal trends for Bayesian posterior parameter estimates generated with fixed-in-time (circles) or T-based (solid squares) priors, taken as an ensemble average over the entire sampling period. Error bars were omitted from each plot for clarity. Figure 7f contains the isotope disequilibrium $\mathcal{D} = \delta_A - \delta_R$.

parameter estimation scenario would be in agreement. Given the importance of these parameters in reconciling global carbon budgets, large uncertainties in them are unacceptable.

[64] Figure 4c shows that the temperature sensitivity of $F_R$ is dependent on the choice of prior values used in the Bayesian parameter estimation routine. This sensitivity to prior values is confirmed by examining the posterior correlation matrix (Figure 5). This means that isotope flux partitioning, when combined with Bayesian parameter estimation, either 1) provides no information about the sensitivity of nonfoliar respiration to temperature, or 2) provides evidence that nonfoliar respiration is controlled by factors other than temperature (such as soil moisture, substrate quality, phenology, etc.).

[65] Sensitivity to prior values is enhanced when there are exactly as many independent observations as unknowns (which is true for a given half hour in equation (14)). Estimates of $\mathcal{D}$ derived from Bayesian parameter estimates of $\Delta_{canopy}$ suggest that the posterior isotopic disequilibrium (Figure 7f) at Niwot Ridge forest is near zero [*Ogée et al.* [2004]]. If this is the case, the system of equations is close to being underdetermined with equation (2) being a multiple of equation (1), and hence is especially sensitive to prior parameter values. This conclusion is also supported with Figure 5 and in addition shows that it is difficult to independently estimate $\delta_N$ and $\beta$ from the data.

### 5.2. Evaluation of Bayesian Parameter Estimation for Isotope Flux Partitioning

#### 5.2.1. Limitations of the Isotope Flux Partitioning Method

[66] There are at least four potential limitations to the isotope flux partitioning method that prevent its use to estimate $F_A$ and $F_R$ on a sub-daily timescale. First, as previously discussed, the isotopic content of the photosynthetic flux may be similar to the isotopic content of the respiratory flux ($\mathcal{D} = 0$) in some (or most) ecosystems [*Bowling et al.*, 2001; *Ogée et al.*, 2003b]. *Ogée et al.* [2003b] and *Baldocchi and Bowling* [2003] suggested that $\mathcal{D}$ is non-zero in midafternoon, allowing for the possibility of a time-varying $\mathcal{D}$ that permits partitioning during at least part of the day. This study strongly supports this claim as Figure 7f shows the highest disequilibrium around midday.

[67] The second limitation of isotope flux partitioning is accurate determination of net ecosystem exchange of $^{13}CO_2$, or the isoflux ($F_\delta$, see equation (2)), which cannot be measured directly at present. The isoflux has been estimated with a variety of techniques (eddy covariance/flask [*Bowling et al.*, 1999a, 2001; *Ogée et al.*, 2003b], HREA [*Bowling et al.*, 1999b], flux-gradient [*Yakir and Wang*, 1996; *Bowling et al.*, 2003a], flux-ratio [*Griffis et al.*, 2004], or biophysical models [*Baldocchi and Bowling*, 2003; *Ogée et al.*, 2003b]). Any one of these techniques can be combined with measurements of $[CO_2]$ and $\delta^{13}C$ to serve as a proxy for $F_\delta$. *Bowling et al.* [2003a] directly compared eddy covariance/flask, HREA, and the flux-gradient techniques in the same study and found convergent results. However, until direct measurement of the $^{13}CO_2$ flux can be done, we must be critical of the uncertainties of each method. If direct measurement of $F_\delta$ were possible by eddy covariance measurements of $^{13}CO_2$ flux [*Saleska et al.*, 2006], this would eliminate estimation of $\delta_N$ and $\beta$ and potentially improve our ability to resolve $F_A$, $F_R$, and $\Delta_{canopy}$ from the data. We examined how better measurements of the isoflux could potentially improve our results by reducing the uncertainty of $F_{isostorage}$ by decreasing the prior standard deviations of $\delta_N$ and $\beta$ by a factor of 10. The posterior correlation matrix showed an improvement in the data to independently determine $F_R$ and $\Delta_{canopy}$, however correlations between $F_A$ and $F_R$ and $F_A$ and $\Delta_{canopy}$ still existed (results not shown).

[68] A third limitation concerns scaling of leaf-level quantities to the canopy. Despite the fundamental importance of $\Delta_{canopy}$ and $\mathcal{D}$, our results do not provide a clear understanding of the nature of these parameters at the

ecosystem scale. At the leaf-level, equations describing $\Delta_{canopy}$ have been extensively studied [*Farquhar et al.*, 1982]. In the absence of biophysical models [*Baldocchi and Bowling*, 2003; *Ogée et al.*, 2003a] that account for leaf-level scaling to the canopy, it is unknown whether or not the same leaf-level relationship for $\Delta_{canopy}$ holds at the ecosystem level. Given the discrepancy between the sign of the isotopic disequilibrium ($\mathcal{D} > 0$ for isotope partitioning studies, $\mathcal{D} < 0$ for leaf-level or global-based modeling studies), more work needs to be done to investigate scaling assumptions and estimation of $\Delta_{canopy}$. If we had a better experimental understanding of $\Delta_{canopy}$, then the prior value could be better constrained and we might have more confidence in our results.

[69] A final limitation of isotope flux partitioning is that accurate estimation of the overall canopy conductance ($\overline{g}$, defined by equation (8)) is critical for a successful partitioning exercise. This was first noted in *Bowling et al.* [2001], who used a form of $\overline{g}$ that did not include diffusion in the mesophyll to the sites of photosynthesis. *Ogée et al.* [2003b] demonstrated the value of incorporating mesophyll conductance in the equation for $\overline{g}$. By including these effects, *Knohl and Buchmann* [2005] have been able to isotopically partition $F$ into $F_A$ and $F_R$ for a two-week timeseries. We would expect mesophyll conductance ($g_m$) to vary in time. However measurements of $g_m$ are difficult to make and hence the diurnal or seasonal variation in $g_m$ is not well known [*Warren and Adams*, 2006; *Warren*, 2006].

#### 5.2.2. Limitations of the Application of Bayesian Parameter Estimation to Isotope Flux Partitioning

[70] In addition to the limitations of the isotope flux partitioning method, there are limitations of the application of the Bayesian parameter estimation method applied to isotope flux partitioning. As shown in section 5.1 the approach of *Ogée et al.* [2004] was expanded by estimating $\Delta_{canopy}$, $\delta_N$, and $\beta$ in addition to $F_A$ and $F_R$. However in spite of these refinements, the Bayesian parameter estimation did not show an improvement in our ability to independently estimate parameters from this data (Figure 5).

[71] Isotope flux partitioning estimates can potentially be used to determine ecosystem-scale functional relationships. Our Bayesian-generated estimates (Figure 4e) produced results basically indistinguishable from the statistical (Figure 4c) or isotope (Figure 4d) non-Bayesian flux partitioning methods. Examining Bayesian parameter estimates derived from fixed-in-time priors generates an interesting result. Bayesian parameter estimates of $F_R$ were sensitive to temperature only when the prior values for $F_R$ were temperature based (Figure 4c). If temperature is the fundamental control on nonfoliar respiration for this ecosystem, then clearly isotope flux partitioning does not work. However, if the isotope partitioning method is correct, then a simplistic temperature dependence for nonfoliar respiration cannot be correct for this subalpine forest.

[72] Figure 6 compares how well the different flux partitioning routines reproduce measured $F$ (Figures 6a and 6b) or $F_\delta$ (Figure 6c). In general, Bayesian parameter estimation was able to reproduce $F$ more than $F_\delta$ as evidenced by the higher $r$ value for $F$ when comparing measured to estimated $F$ and $F_\delta$. This result is also indicative of our ability to measure $F$ with far more confidence than $F_\delta$.

[73] The lack of multiple, independent equations describing $F_A$, $F_R$ and $\Delta_{canopy}$ is a mathematical limitation to the isotope partitioning method. Because of this, Bayesian parameter estimates are highly sensitive to prior parameter values. This limitation has previously been noted [*Ogée et al.*, 2004], and one suggestion was that inclusion of oxygen isotope measurements ($\delta^{18}O$ of $CO_2$) can help constrain parameter estimates of $F_A$ and $F_R$ [*Yakir and Wang*, 1996]. Concurrent measurements of $\delta^{18}O$ data were not made in this study. Using Bayesian parameter estimation to estimate a single daily value of the target parameters is one way to test whether multiple, independent measurements can reduce the sensitivity to prior parameters. The posterior correlation matrix $E$ from daily parameter estimation had a similar structure as Figure 5, and hence the results are not shown in this study. When isotope flux partitioning is compared to statistical regressions of temperature and $F$, over the course of a night, as many as 15 independent paired measurements of $F$ and air temperature are used to determine an exponential relationship that can have as few as two parameters [*Reichstein et al.*, 2005a].

[74] We expect posterior estimates of $F_A \leq 0$ and $F_R \geq 0$, however, some half-hourly periods generated results that produced non-sensible results of $F_R < 0$ (Figure 3e). We note that some of these time periods where $F_R < 0$ also occurred for the non-Bayesian isotope flux partitioning estimates of $F_A$ and $F_R$ (Figure 3d). This suggests examination of the isotope partitioning model to determine what causes this discrepancy in sign, as the Appendix in *Bowling et al.* [2001] showed that solutions of the isotope partitioning model yields a unique estimate for the fluxes. Non-sensible Bayesian posterior estimates are also influenced by the assumption that the prior distributions of $F_A$ and $F_R$ are normal. Mathematically, a normally distributed random variable has no sign restrictions. If the prior mean value is close to zero with a large variance, it is entirely feasible (but biologically meaningless) that the Bayesian parameter estimate be of opposite sign than expected. This limitation could be overcome with the implementation of biophysically realistic prior distributions for $F_A$ and $F_R$.

[75] Three modifications to the Bayesian parameter estimation method could take additional advantages of the information contained in high-resolution measurements of $F$, [$CO_2$] and $\delta^{13}C$. First, the model could be constrained by assuming that parameters (namely $F_A$ and $F_R$) vary smoothly in time under some given model and apply techniques such as a Kalman filter to estimate parameters [*Peters et al.*, 2005; *Gove and Hollinger*, 2006]. This effectively reduces the number of degrees of freedom and helps to constrain the target parameters. Second, different assumptions on the probability distributions of the prior parameter values and data could prevent non-sensible Bayesian parameter estimates (e.g., lognormally distributed $F_A$ and $F_R$ would prevent Bayesian estimates of $F_A > 0$ and $F_R < 0$). Third, different process models could be used to constrain the fluxes to environmental variables (e.g., $F_R$ functionally dependent on soil temperature, soil moisture, plant phenology, etc.). These modifications might require the use of Monte Carlo techniques to simulate posterior parameter distributions [*Gelman et al.*, 1995; *Knorr and Kattge*, 2005; *Braswell et al.*, 2005; *Sacks et al.*, 2006; *Xu et*

*al.*, 2006], as the analytical Bayesian parameter estimate (equations (17) and (18)) might not hold.

[76] The success and further development of the isotope flux partitioning method will require advances in understanding in several areas. Isotope partitioning results are likely to be substantially improved with greater understanding of (a) the isotopic signature of daytime nonfoliar respiration and (b) isotopic disequilibrium, particularly with regard to resolving conflicting estimates of $\mathcal{D}$ in ecosystem and global scale studies. Application of the isotope partitioning method in ecosystems expected to show larger disequilibrium (e.g., a mixed $C_3$–$C_4$ ecosystem) and investigation of seasonal variation in $\mathcal{D}$ in contrasting biomes would elucidate how environmental variation and phenology influence $\mathcal{D}$. Such studies may lead to important new understanding of the magnitude of the inferred terrestrial carbon sink [*Randerson et al.*, 2002]. There is also a direct need to understand diurnal variation and ecosystem-scale importance of (a) mesophyll conductance [*Warren*, 2006; *Warren and Adams*, 2006] and (b) post-photosynthetic fractionations [*Ghashghaie et al.*, 2003; *Tcherkez et al.*, 2003; *Badeck et al.*, 2005; *Tcherkez and Farquhar*, 2005; *Nogués et al.*, 2006]. Such studies will improve our overall knowledge of ecosystem-scale isotopic processes, and as a result will improve the overall effectiveness of isotope flux partitioning.

## 6. Conclusions

[77] A Bayesian optimization method was combined with an isotopic partitioning method to examine the fluxes of net photosynthesis and nonfoliar respiration in a high-elevation subalpine forest in Colorado. Results were generally consistent with fluxes obtained from statistical regression methods between fluxes and climatic variables, including the methods of *Yi et al.* [2004] and *Reichstein et al.* [2005a]. However, examination of the posterior correlation matrix revealed that the data were not able to independently resolve all the parameters.

[78] The results of this study confirm the conclusions of *Ogée et al.* [2004] that (a) a small disequilibrium between $F_A$ and $F_R$ limits the effectiveness of isotope flux partitioning on a diurnal timescale by generating unacceptable uncertainties for $F_A$ and $F_R$, (b) poor characterization of key parameters (whole-canopy photosynthetic discrimination, mesophyll conductance, and the isoflux) and (c) the lack of independent multiple observations prevent effective implementation of the Bayesian approach. These results are supported with the large density of data even when bin-averaged into mean diurnal patterns. We advocate that future isotope flux partitioning studies address and investigate these limitations through (a) utilization of additional measurements (such as $C^{18}O^{16}O$ measurements) and (b) better characterization of $\delta_R$ during the daytime in order to improve upon the isotope flux partitioning method.

## Appendix A: Bayesian Parameter Estimation of Daytime Isotopic Mixing Relationships

[79] Here we provide an example to illustrate the Bayesian approach. We focus solely on parameters for daytime isotopic mixing relationships (namely $\delta_N$ and $\beta$). Furthermore isotopic mixing lines can be characterized as a linear Bayesian parameter estimation problem, facilitating their analysis. For this example we demonstrate how to set up and calculate the fundamental components to a Bayesian parameter estimation problem (e.g., equations (17) and (18)). The $[CO_2]$ and $\delta^{13}C$ data utilized for this example are shown in Figure 2b.

[80] Equation (5) gives a functional relationship between measurements of $[CO_2]$ and $\delta^{13}C$ to mixing line parameters $\delta_N$ and $\beta$. *Zobitz et al.* [2006] showed that because $[CO_2]$ is measured more precisely than $\delta^{13}C$, $\delta_N$ uncertainty is influenced more by $\delta^{13}C$ uncertainties than $[CO_2]$ measurement uncertainty. This assumption allows for the estimation of $\delta_N$ and $\beta$ to be characterized as a linear parameter estimation problem. (See *Tarantola* [2005, p. 273] for an example if $[CO_2]$ and $\delta^{13}C$ both had measurement uncertainties.)

[81] For this study, $[CO_2]$ and $\delta^{13}C$ were measured at nine different heights. Hence the model relating the parameters to the data is the following matrix equation:

$$\begin{bmatrix} 1 & 1/C_1 \\ 1 & 1/C_2 \\ 1 & 1/C_3 \\ 1 & 1/C_4 \\ 1 & 1/C_5 \\ 1 & 1/C_6 \\ 1 & 1/C_7 \\ 1 & 1/C_8 \\ 1 & 1/C_9 \end{bmatrix} \begin{bmatrix} \delta_N \\ \beta \end{bmatrix} = \begin{bmatrix} \delta_1 \\ \delta_2 \\ \delta_3 \\ \delta_4 \\ \delta_5 \\ \delta_6 \\ \delta_7 \\ \delta_8 \\ \delta_9 \end{bmatrix} \tag{A1}$$

$$G\vec{m} = \vec{d}, \tag{A2}$$

where for convenience $C_i$ and $\delta_i$ represents a measurement of $[CO_2]$ and $\delta^{13}C$. We make the assumption that each measurement of $\delta^{13}C$ is independent and uncorrelated to the other measurements and is normally distributed about $\delta_i$ with standard deviation 0.15‰. Hence, the covariance matrix is a diagonal matrix:

$$C_D = \begin{bmatrix} \sigma_\delta^2 & 0 & 0 & 0 & 0 & 0 & 0 & 0 & 0 \\ 0 & \sigma_\delta^2 & 0 & 0 & 0 & 0 & 0 & 0 & 0 \\ 0 & 0 & \sigma_\delta^2 & 0 & 0 & 0 & 0 & 0 & 0 \\ 0 & 0 & 0 & \sigma_\delta^2 & 0 & 0 & 0 & 0 & 0 \\ 0 & 0 & 0 & 0 & \sigma_\delta^2 & 0 & 0 & 0 & 0 \\ 0 & 0 & 0 & 0 & 0 & \sigma_\delta^2 & 0 & 0 & 0 \\ 0 & 0 & 0 & 0 & 0 & 0 & \sigma_\delta^2 & 0 & 0 \\ 0 & 0 & 0 & 0 & 0 & 0 & 0 & \sigma_\delta^2 & 0 \\ 0 & 0 & 0 & 0 & 0 & 0 & 0 & 0 & \sigma_\delta^2 \end{bmatrix} \tag{A3}$$

[82] If measurements of $\delta^{13}C$ were correlated with each other, then off-diagonal terms in equation (A3) would arise. The prior mean value and standard deviation for $\delta_N$ and $\beta$ from Table 3 can be organized into the vector $\vec{m}_{prior}$ and $C_M$ assuming that prior values $\delta_N$ and $\beta$ are normally distributed:

$$\vec{m}_{prior} = \begin{bmatrix} -24.5 \\ 6100 \end{bmatrix} \tag{A4}$$

$$C_M = \begin{bmatrix} 10^2 & 0 \\ 0 & 1000^2 \end{bmatrix}. \tag{A5}$$

[83] Similar to $C_D$, we assume there is no a priori correlation between $\delta_N$ and $\beta$, hence diagonal elements of $C_M$ are zero. Using the data in Figure 2b, the posterior Bayesian parameter estimate and covariance matrix can be calculated with equations (17) and (18):

$$\vec{m}_* = \begin{bmatrix} -24.2 \\ 6004 \end{bmatrix} \tag{A6}$$

$$\tilde{C}_M = \begin{bmatrix} 2.5^2 & -2352 \\ -2352 & 942^2 \end{bmatrix}. \tag{A7}$$

[84] Since the off-diagonal terms in $\tilde{C}_M$ are non-zero, parameter estimates are correlated. The degree that these estimates are correlated can be found from the posterior correlation matrix, whose off diagonal term is $-0.99$. The best fit line using the values of $\vec{m}_*$ as shown as a dashed line in Figure 2b.

[85] **Acknowledgments.** J.M.Z. would like to acknowledge David Dobson, Frederick Adler, and James Keener for providing insightful comments into the Bayesian parameter estimation method. The authors gratefully acknowledge three anonymous reviewers, Philippe Peylin, Sean Schaeffer, and Andrew Moyes for improving previous versions of the manuscript; Bill Smith for discussions on mesophyll conductance; Chuixiang Xi for sharing data; and Russ Monson for providing data from the Niwot Ridge AmeriFlux tower. This work was funded by the University of Utah and a grant to D.R.B. from the Office of Science (BER), U.S. Department of Energy, grant DE-FG02-04ER63904 as part of the North American Carbon Program. J.M.Z. was funded through NSF grant DGE-0217424 and as a fellow in the U.S. Department of Energy, Global Change Education Program, administered by the Oak Ridge Institute for Science and Education. Additional funding supported by the Modeling the Dynamics of Life Fund and The Department of Mathematics at the University of Utah. An online version of the statistical flux partitioning algorithm is available at http://gaia.agraria.unitus.it/database/eddyproc/.

## References

Aber, J. D., P. B. Reich, and M. L. Goulden (1996), Extrapolating leaf $CO_2$ exchange to the canopy: a generalized model of forest photosynthesis compared with measurements by eddy correlation, *Oecologia*, *106*, 257–265.

Aranibar, J. N., J. A. Berry, W. J. Riley, D. E. Pataki, B. E. Law, and J. R. Ehleringer (2006), Combining meterology, eddy fluxes, isotope measurements, and modeling to understand environmental controls of carbon isotope discrimination at the canopy scale, *Global Change Biol.*, *12*, 710–730, doi:10.1111/j.1365-2486.2006.01121.x.

Badeck, F. W., G. Tcherkez, S. Nogués, C. Piel, and J. Ghashghaie (2005), Post-photosynthetic fractionation of stable carbon isotopes between plant organs-a widespread phenomeonon, *Rapid Commun. Mass Spectrom.*, *19*, 1381–1391, doi:10.1002/rcm.1912.

Baldocchi, D. D., and D. R. Bowling (2003), Modelling the discrimination of $^{13}CO_2$ above and within a temperate broad-leaved forest canopy on hourly to seasonal time scales, *Plant Cell Environ.*, *26*, 231–244.

Baldocchi, D., et al. (2001), FLUXNET: A New Tool to Study the Temporal and Spatial Variability of Ecosystem-Scale Carbon Dioxide, Water Vapor, and Energy Flux Densities, *Bull. Am. Meterol. Soc.*, *82*(11), 2415–2434.

Bousquet, P., P. Ciais, P. Peylin, M. Ramonet, and P. Monfray (1999), Inverse modeling of annual atmospheric $CO_2$ sources and sinks: 1. Method and control inversion, *J. Geophys. Res.*, *104*(D21), 26,161–26,178.

Bowling, D. R., D. D. Baldocchi, and R. K. Monson (1999a), Dynamics of isotopic exchange of carbon dioxide in a tennessee deciduous forest, *Global Biogeochem. Cycles*, *13*(4), 903–922.

Bowling, D. R., A. C. Delany, A. A. Turnipseed, and D. D. Baldocchi (1999b), Modification of the relaxed eddy accumulation technique to maximize measured scalar mixing ratio differences in updrafts and downdrafts, *J. Geophys. Res.*, *104*(D8), 9121–9133.

Bowling, D. R., P. P. Tans, and R. K. Monson (2001), Partitioning net ecosystem carbon exchange with isotopic fluxes of $CO_2$, *Global Change Biol.*, *7*, 127–145.

Bowling, D. R., D. E. Pataki, and J. R. Ehleringer (2003a), Critical evaluation of micrometerological methods for measuring ecosystem-atmosphere isotopic exchange of $CO_2$, *Agric. For. Meteorol.*, *116*, 159–179.

Bowling, D. R., S. D. Sargent, B. D. Tanner, and J. R. Ehleringer (2003b), Tunable diode laser absorption spectroscopy for ecosystem-atmosphere $CO_2$ isotopic exchange studies, *Agric. For. Meteorol.*, *118*, 1–19.

Bowling, D. R., S. P. Burns, T. J. Conway, R. K. Monson, and J. W. C. White (2005), Extensive observations of $CO_2$ carbon isotope content in and above a high-elevation subalpine forest, *Global Biogeochem. Cycles*, *19*, GB3023, doi:10.1029/2004GB002394.

Braswell, B. H., W. J. Sacks, E. Linder, and D. S. Schimel (2005), Estimating diurnal to annual ecosystem parameters by synthesis of a carbon flux model with eddy covariance net ecosystem exchange observations, *Global Change Biol.*, *11*, 335–355, doi:10.1111/j.1365-2486.2005.00897.x.

Ciais, P., P. P. Tans, J. W. C. White, M. Trolier, R. J. Francey, J. A. Berry, D. R. Randall, P. J. Sellers, J. G. Collatz, and D. S. Schimel (1995), Partitioning of ocean and land uptake of $CO_2$ as inferred by $\delta^{13}C$ measurements from the NOAA Climate Monitoring and Diagnostics Laboratory Global Air Sampling Network, *J. Geophys. Res.*, *100*(D3), 5051–5070.

Ciais, P., et al. (2005), Europe-wide reduction in primary productivity caused by the heat and drought in 2003, *Nature*, *437*, 529–533, doi:10.1038/nature03972.

Clark, J. S. (2005), *Models for Ecological Data: Statistical Computation for Classical and Bayesian Approaches*, Princeton Univ. Press, Princeton, N. J.

Dai, Y., R. E. Dickinson, and Y. Ping Wang (2004), A two-big-leaf model for canopy temperature, photosynthesis, and stomatal conductance, *J. Clim.*, 2281–2299.

Dang, Q. L., H. A. Margolis, M. Sy, M. R. Coyea, G. J. Collatz, and C. L. Walthall (1997), Profiles of photosynthetically active radiation, nitrogen and photosynthetic capacity in the boreal forest: Implications for scaling from leaf to canopy, *J. Geophys. Res.*, *102*(D24), 28,845–28,859.

Davidson, E. A., and I. A. Janssens (2006), Temperature sensitivity of soil carbon decomposition and feedbacks to climate change, *Nature*, *440*, 165–173, doi:10.1038/nature04514.

Davidson, E. A., I. A. Janssens, and Y. Luo (2006), On the variability of respiration in terrestrial ecosystems: moving beyond $Q_{10}$, *Global Change Biol.*, *12*, 154–164, doi:10.1111/j.1365-2486.2005.01065.x.

Farquhar, G. D., and J. Lloyd (1993), Carbon and oxygen isotope effects in the exchange of carbon dioxide between terrestrial plants and the atmosphere, in *Stable Isotopes and Plant Carbon-Water Relations*, vol. 40, edited by J. R. Ehleringer, A. E. Hall, and G. D. Farquhar, pp. 47–70, Academic, San Diego, Calif.

Farquhar, G. D., M. H. O'Leary, and J. A. Berry (1982), On the relationship between carbon isotope discrimination and the intracellular carbon dioxide concentration in leaves, *Aust. J. Plant Physiol.*, *9*, 121–137.

Farquhar, G. D., J. R. Ehleringer, and K. T. Hubick (1989), Carbon isotope discrimination and photosynthesis, *Annu. Rev. Plant Physiol. Plant Mol. Biol.*, *40*, 503–537.

Francey, R. J., C. E. Allison, D. M. Etheridge, C. M. Trudinger, I. G. Enting, M. Leuenberger, R. L. Langenfelds, E. Michel, and L. P. Steele (1999), A 1000-year high precision record of $\delta^{13}C$ in atmospheric $CO_2$, *Tellus*, *51B*, 170–193.

Fung, I., et al. (1997), Carbon 13 exchanges between the atmosphere and biosphere, *Global Biogeochem. Cycles*, *11*(4), 507–533.

Gelman, A., J. B. Carlin, H. S. Stern, and D. B. Rubin (1995), *Bayesian Data Analysis*, Chapman and Hall, London, UK.

Ghashghaie, J., F. W. Badeck, G. Lanigan, S. Nogués, G. Tcherkez, E. Deléens, G. Cornic, and H. Griffiths (2003), Carbon isotope fractionation during dark respiration and photorespiration in $C_3$ plants, *Phytochem. Rev.*, *2*, 145–161.

Giardina, C. P., and M. G. Ryan (2000), Evidence that decomposition rates of organic carbon in mineral soil do not vary with temperature, *Nature*, *404*, 858–861.

Goulden, M. L., J. W. Munger, S. M. Fan, B. C. Daube, and S. C. Wofsy (1996), Exchange of carbon dioxide by a deciduous forest: response to interannual climate variability, *Science*, *271*, 1576–1578.

Gove, J. H., and D. Y. Hollinger (2006), Application of a dual unscented Kalman filter for simultaneous state and parameter estimation in problems of surface-atmosphere exchange, *J. Geophys. Res.*, *111*, D08S07, doi:10.1029/2005JD006021.

Grace, J., J. Lloyd, J. McIntyre, A. Miranda, P. Meir, H. Miranda, J. Moncrieff, J. Massheder, I. Wright, and J. Gash (1995), Fluxes of carbon dioxide and water vapour over an undisturbed tropical forest in south-west Amazonia, *Global Change Biol.*, *1*, 1–12.

Greco, S., and D. D. Baldocchi (1996), Seasonal variations of $CO_2$ and water vapour exchange rates over a temperate deciduous forest, *Global Change Biol.*, *2*, 183–197.

Griffis, T. J., J. M. Baker, S. D. Sargent, B. D. Tanner, and J. Zhang (2004), Measuring field-scale isotopic $CO_2$ fluxes with tunable diode laser absorption spectroscopy and micrometerological techniques, *Agric. For. Meteorol.*, *124*, 15–29.

Griffis, T. J., J. M. Baker, and J. Zhang (2005), Seasonal dynamics and partitioning of isotopic $CO_2$ exchange in a $C_3/C_4$ managed ecosystem, *Agric. For. Meteorol.*, *132*, 1–19.

Gubbins, D. (2004), *Time Series Analysis and Inverse Theory for Geophysicists*, Cambridge Univ. Press, Cambridge, UK.

Huxman, T. E., A. A. Turnipseed, J. P. Sparks, P. C. Harley, and R. K. Monson (2003), Temperature as a control over ecosystem $CO_2$ fluxes in a high-elevation, subalpine forest, *Oecologia*, *134*, 537–546.

Hymus, G. J., K. Maseyk, R. Valentinil, and D. Yakir (2005), Large daily variation in $^{13}$C-enrichment of leaf-respired $CO_2$ in two Quercus forest canopies, *New Phytol.*, *167*, 377–384, doi:10.1111/j.1469-8137.2005.01475.x.

Janssens, I. A., et al. (2001), Productivity overshadows temperature in determining soil and ecosystem respiration across European forests, *Global Change Biol.*, *7*, 269–278.

Jaynes, E. T. (2003), *Probability Theory: The Logic of Science*, Cambridge Univ. Press, Cambridge, UK.

Keeling, C. (1958), The concentrations and isotopic abundances of atmospheric carbon dioxide in rural areas, *Geochim. Cosmochim. Acta*, *13*, 322–334.

Knohl, A., and N. Buchmann (2005), Partitioning the net $CO_2$ flux of a deciduous forest into respiration and assimilation using stable carbon isotopes, *Global Biogeochem. Cycles*, *19*, GB4008, doi:10.1029/2004GB002301.

Knorr, W., and J. Kattge (2005), Inversion of terrestrial ecosystem model parameter values against eddy covariance measurements by Monte Carlo sampling, *Global Change Biol.*, *11*, 1333–1351, doi:10.1111/j.1365-2486.2005.00977.x.

Lai, C. T., J. R. Ehleringer, P. P. Tans, S. C. Wofsy, S. P. Urbanski, and D. Y. Hollinger (2004), Estimating photosynthetic $^{13}$C discrimination in terrestrial $CO_2$ exchange from canopy to regional scales, *Global Biogeochem. Cycles*, *18*, GB1041, doi:10.1029/2003GB002148.

Lai, C. T., J. R. Ehleringer, A. J. Schauer, P. P. Tans, D. Y. Hollinger, K. T. Paw U, J. W. Munger, and S. C. Wofsy (2005), Canopy-scale $\delta^{13}$C of photosynthetic and respiratory $CO_2$ fluxes: observations in forest biomes across the United States, *Global Change Biol.*, *11*, 633–643, doi:10.1111/j.1365-2486.2005.00931.x.

Lavigne, M. B., et al. (1997), Comparing nocturnal eddy covariance measurements to estimates of ecosystem respiration made by scaling chamber measurements at six coniferous boreal sites, *J. Geophys. Res.*, *102*(D24), 28,977–28,985.

Law, B. E., M. G. Ryan, and P. M. Anthoni (1999), Seasonal and annual respiration of a ponderosa pine ecosystem, *Global Change Biol.*, *5*, 169–182.

Lloyd, J., and J. A. Taylor (1994), On the temperature dependence of soil respiration, *Functional Ecol.*, *8*, 315–323.

Lloyd, J., et al. (1996), Vegetation effects on the isotopic composition of atmospheric $CO_2$ at local and regional scales: Theoretical aspects and a comparison between rain forest in Amazonia and a boreal forest in Siberia, *Aust. J. Plant Physiol.*, *23*, 371–399.

Miller, J. B., P. P. Tans, J. W. C. White, T. J. Conway, and B. W. Vaughn (2003), The atmospheric signal of terrestrial carbon isotopic discrimination and its implication for partitioning carbon fluxes, *Tellus*, *55B*, 197–206.

Monson, R. K., A. A. Turnipseed, J. P. Sparks, P. C. Harley, L. E. Scott Denton, K. Sparks, and T. E. Huxman (2002), Carbon sequestration in a high-elevation, subalpine forest, *Global Change Biol.*, *8*, 459–478.

Monson, R. K., D. L. Lipson, S. P. Burns, A. A. Turnipseed, A. C. Delany, M. W. Williams, and S. K. Schmidt (2006), Winter forest soil respiration controlled by climate and microbial community composition, *Nature*, *439*, 711–714, doi:10.1038/nature04555.

Nogués, S., C. Damesin, G. Tcherkez, F. Maunoury, G. Cornic, and J. Ghashghaie (2006), $^{13}$C/$^{12}$C isotope labelling to study leaf carbon respiration and allocation in twigs of field-grown beech trees, *Rapid Commun. Mass Spectrom.*, *20*, 219–226, doi:10.1002/rcm.2297.

Ogée, J., et al. (2003a), MuSICA, a $CO_2$, water and energy multilayer, multileaf pine forest model: evaluation from hourly to yearly time scales and sensitivity analysis, *Global Change Biol.*, *9*, 697–717.

Ogée, J., P. Peylin, P. Ciais, T. Bariac, Y. Brunet, P. Berbigier, C. Roche, P. Richard, G. Bardoux, and J. M. Bonneford (2003b), Partitioning net ecosystem carbon exchange into net assimilation and respiration using $^{13}CO_2$ measurements: A cost-effective sampling strategy, *Global Biogeochem. Cycles*, *17*(2), 1070, doi:10.1029/2002GB001995.

Ogée, J., P. Peylin, M. Cuntz, T. Bariac, Y. Brunet, P. Berbigier, P. Richard, and P. Ciais (2004), Partitioning net ecosystem carbon exchange into net assimilation and respiration with canopy-scale isotopic measurements: An error propagation analysis with $^{13}CO_2$ and $CO^{18}O$ data, *Global Biogeochem. Cycles*, *18*, GB2019, doi:10.1029/2003GB002166.

Pataki, D. E., J. R. Ehleringer, L. B. Flanagan, D. Yakir, D. R. Bowling, C. J. Still, N. Buchmann, J. O. Kaplan, and J. Berry (2003), The application and interpretation of Keeling plots in terrestrial carbon cycle research, *Global Biogeochem. Cycles*, *17*(1), 1022, doi:10.1029/2001GB001850.

Pataki, D. E., D. R. Bowling, J. R. Ehleringer, and J. M. Zobitz (2006), High resolution atmospheric monitoring of urban carbon dioxide sources, *Geophys. Res. Lett.*, *33*, L03813, doi:10.1029/2005GL024822.

Peters, W., J. B. Miller, J. Whitaker, A. S. Denning, A. Hirsch, M. C. Krol, D. Zupanski, L. Bruhwiler, and P. P. Tans (2005), An ensemble data assimilation system to estimate $CO_2$ surface fluxes from atmospheric trace gas observations, *J. Geophys. Res.*, *110*, D24304, doi:10.1029/2005JD006157.

Piovesan, G., and J. M. Adams (2000), Carbon balance gradient in European forests: interpreting EUROFLUX, *J. Vegetation Sci.*, *11*, 923–926.

Prater, J. L., B. Mortazavi, and J. P. Chanton (2006), Diurnal variation of the $\delta^{13}C$ of pine needle respired $CO_2$ evolved in darkness, *Plant Cell Environ.*, *29*, 202–211.

Randerson, J. T., G. J. Collatz, J. E. Fessenden, A. D. Munoz, C. J. Still, J. A. Berry, I. Y. Fung, N. Suits, and A. S. Denning (2002), A possible global covariance between terrestrial gross primary production and $^{13}$C discrimination: Consequences for the atmospheric $^{13}$C budget and its response to ENSO, *Global Biogeochem. Cycles*, *16*(4), 1136, doi:10.1029/2001GB001845.

Raupach, M. R. (2001), Inferring biogeochemical sources and sinks from atmospheric concentrations: General considerations and applications in vegetation canopies, in *Global Biogeochemical Cycles in the Climate System*, edited by E.-D. Schulze et al., chap. 1.4, pp. 41–59, Academic, San Diego, Calif.

Raupach, M. R., P. J. Rayner, D. J. Barrett, R. S. DeFries, M. Heimann, D. S. Ojima, S. Quegan, and C. C. Schmullius (2005), Model-data synthesis in terrestrial carbon observation: methods, data requirements and data uncertainty specifications, *Global Change Biol.*, *11*, 378–397, doi:10.1111/j.1365-2486.2005.00917.x.

Reichstein, M., et al. (2005a), On the separation of net ecosystem exchange into assimilation and ecosystem respiration: review and improved algorithm, *Global Change Biol.*, *11*, 1424–1439, doi:10.1111/j.1365-2486.2005.001002.x.

Reichstein, M., T. Kätterer, O. Andrén, P. Ciais, E. D. Schulze, W. Cramer, D. Papale, and R. Valentini (2005b), Temperature sensitivity of decomposition in relation to soil organic matter pools: critique and outlook, *Biogeosciences*, *2*, 317–321.

Sacks, W. J., D. S. Schimel, R. K. Monson, and B. H. Braswell (2006), Model-data synthesis of diurnal and seasonal $CO_2$ fluxes at Niwot Ridge, Colorado, *Global Change Biol.*, *12*, 240–259, doi:10.1111/j.1365-2486.2005.01059.x.

Saleska, S., J. Shorter, S. Herndon, R. Jimenez, B. McManus, W. Munger, D. Nelson, and M. Zahniser (2006), What are the instrumentation requirements for measuring the isotopic composition of net ecosystem exchange of $CO_2$ using eddy covariance methods?, *Isotopes Environ. Health Stud.*, *42*(2), 115–133.

Scartazza, A., C. Mata, G. Matteucci, D. Yakir, S. Moscatello, and E. Brugnoli (2004), Comparisons of $\delta^{13}$C of photosynthetic products and ecosystem respiratory $CO_2$ and their responses to seasonal climate variability, *Oecologia*, *140*, 340–351.

Schauer, A. J., C. T. Lai, D. R. Bowling, and J. R. Ehleringer (2003), An automated sampler for collection of atmospheric trace gas samples for stable isotope analyses, *Agric. For. Meteorol.*, *118*, 113–124.

Schimel, D. S., et al. (2001), Recent patterns and mechanisms of carbon exchange by terrestrial ecosystems, *Nature*, *414*, 169–172.

Scholze, M., J. O. Kaplan, W. Knorr, and M. Heimann (2003), Climate and interannual variability of the atmosphere-biosphere $^{13}CO_2$ flux, *Geophys. Res. Lett.*, *30*(2), 1097, doi:10.1029/2002GL015631.

Stoy, P. C., G. G. Katul, M. B.S. Siqueira, J. Y. Juang, K. A. Novick, J. M. Uebelherr, and R. Oren (2006), An evaluation of models for partitioning eddy-covariance measured net ecosystem exchange into photosynthesis and respiration, *Agric. For. Meteorol.*, *141*, 2–18.

Suits, N. S., A. S. Denning, J. A. Berry, C. J. Still, J. Kaduk, J. B. Miller, and I. T. Baker (2005), Simulation of carbon isotope discrimination of the terrestrial biosphere, *Global Biogeochem. Cycles*, *19*, GB1017, doi:10.1029/2003GB002141.

Tarantola, A. (2005), *Inverse Problem Theory and Model Parameter Estimation*, SIAM, Philadelphia, Pa.

Tcherkez, G., and G. D. Farquhar (2005), Carbon isotope effect predictions for enzymes involved in the primary carbon metabolism of plant leaves, *Functional Plant Biol.*, *32*, 277–291.

Tcherkez, G., et al. (2003), Metabolic origin of carbon isotope composition of leaf dark-respired $CO_2$ in French bean, *Plant Physiol.*, *131*, 237–244.

Tissue, D. T., M. M. Barbour, J. E. Hunt, M. H. Turnbull, K. L. Griffin, A. S. Walcroft, and D. Whitehead (2006), Spatial and temporal scaling of intercellular $CO_2$ concentration in a temperate rain forest dominated by *Dacrydium cupressinum* in New Zealand, *Plant Cell Environ.*, *26*, 497–510, doi:10.1111/j.1365-3040.2005.01427.x.

Trumbore, S. (2000), Age of soil organic matter and soil respiration: radiocarbon constraints on belowground C dynamics, *Ecol. Appl.*, *10*(2), 399–411.

Turnipseed, A. A., D. E. Anderson, P. D. Blanken, W. M. Baugh, and R. K. Monson (2003), Airflows and turbulent flux measurements in mountainous terrain Part 1. Canopy and local effects, *Agric. For. Meteorol.*, *119*, 1–21.

Valentini, R., et al. (2000), Respiration as the main determinant of carbon balance in European forests, *Nature*, *404*, 861–865.

Van Dijk, A. I. J. M., and A. J. Dolman (2004), Estimates of $CO_2$ uptake and release among European forests based on eddy covariance data, *Global Change Biol.*, *10*, 1445–1459, doi:10.1111/j.1365-2486.2004.00831.

Vogel, J. S. (1980), *Fractionation of Carbon Isotopes During Photosynthesis*, Springer, Heidelberg.

Warren, C. R. (2006), Estimating the internal conductance to $CO_2$ movement, *Functional Plant Biol.*, *33*, 431–442.

Warren, C. R., and M. A. Adams (2006), Internal conductance does not scale with photosynthetic capacity: implications for carbon isotope discrimination and the economics of water and nitrogen use in photosynthesis, *Plant Cell Environ.*, *29*, 192–201.

Webb, E. K., G. I. Pearman, and R. Leuning (1980), Correction of flux measurements for density effects due to heat and water vapour transfer, *Q. J.R. Meteorol. Soc.*, *106*, 127–150.

Wofsy, S. C., M. L. Goulden, J. W. Munger, S. M. Fan, P. S. Bakwin, B. C. Daube, S. L. Bassow, and F. A. Bazzaz (1993), Net exchange of $CO_2$ in a mid-latitude forest, *Science*, *260*, 1314–1317.

Xu, T., L. White, D. Hui, and Y. Luo (2006), Probabilistic inversion of a terrestrial ecosystem model: Analysis of uncertainty in parameter estimation and model prediction, *Global Biogeochem. Cycles*, *20*, GB2007, doi:10.1029/2005GB002468.

Yakir, D. (2004), The stable isotopic composition of atmospheric $CO_2$, in *The Atmosphere: Treatise on Geochemistry*, vol. 4, edited by R. Keeling, chap. 4, pp. 175–212, Elsevier, New York.

Yakir, D., and X.-F. Wang (1996), Fluxes of $CO_2$ and water between terrestrial vegetation and the atmosphere estimated from isotope measurements, *Nature*, *380*, 515–517.

Yi, C., et al. (2004), A nonparametric method for separating photosynthesis and respiration components in $CO_2$ flux measurements, *Geophys. Res. Lett.*, *31*, L17107, doi:10.1029/2004GL020490.

Zhang, J., T. J. Griffis, and J. M. Baker (2006), Using continuous stable isotope measurements to partition net ecosystem $CO_2$ exchange, *Plant Cell Environ.*, *29*, 483–496, doi:10.1111/j.1365-3040.2005.01425.x.

Zobitz, J. M., J. P. Keener, H. Schnyder, and D. R. Bowling (2006), Sensitivity analysis and quantification of uncertainty for isotopic mixing relationships in carbon cycle research, *Agric. For. Meteorol.*, *136*, 56–75, doi:10.1016/j.agrformet.2006.01.003.

D. R. Bowling, Department of Biology, University of Utah, 257 S 1400 E, Salt Lake City, UT 84112, USA.

S. P. Burns, Department of Ecology and Evolutionary Biology (EEB), University of Colorado, Boulder, CO 80309-0334, USA.

J. Ogée, EPHYSE (Functional Ecology and Environmental Physics), INRA, BP 81, F-33883 Villenave d'Ornon, France.

M. Reichstein, Biogeochemical Model-Data Integration Group, Max-Planck Institute for Biogeochemistry, Hans-Knöll-Str. 10, 07745 Jena, Germany.

J. M. Zobitz, Department of Mathematics, University of Utah, 155 S 1400 E, Salt Lake City, UT 84112, USA. (zobitz@math.utah.edu)